OPEN ACCESS

Scholars International Journal of Chemistry and Material Sciences

Abbreviated Key Title: Sch Int J Chem Mater Sci
ISSN 2616-8669 (Print) |ISSN 2617-6556 (Online)
Scholars Middle East Publishers, Dubai, United Arab Emirates
Journal homepage: http://saudijournals.com

Review Article

AI-Guided Single-Atom Electrocatalysts for Carbon-Neutral Chemical Manufacturing: from CO_2 Conversion to Green Ammonia Synthesis

Swaira Anjum[1], Amir Sohail[2], Muhammad Ibrahim[3], Shah Faisal[4], Noman Hassan[5], Muhammad Umer Farooq[6], Muhammad Tariq[7], Waqar Yousaf[8], Umar Farooq[5], Waheed Zaman Khan[9,10]*

[1]Department of Chemistry, Rawalpindi Women University, Rawalpindi 46300, Punjab, Pakistan
[2]Department of Chemistry, University of Malakand, Chakdara, Lower Dir 18800, Khyber Pakhtunkhwa, Pakistan
[3]Department of Physics, University of Sargodha, Sargodha 40100, Punjab, Pakistan
[4]Dalian Institute of Chemical Physics, Chinese Academy of Sciences, Dalian 116023, China
[5]Department of Chemistry, Thal University Bhakkar, Bhakkar 30000, Punjab, Pakistan
[6]Department of Chemistry, University of Engineering and Technology (UET), Lahore 54890, Punjab, Pakistan
[7]Department of Chemistry, Division of Science and Technology, University of Education, Township, Lahore 54770, Punjab, Pakistan
[8]Department of Hydrogen Technology, Rosenheim University of Applied Sciences, Burghausen Campus, 84489 Burghausen, Germany
[9]Department of Physics, Division of Science and Technology, University of Education, College Road, Township, Lahore 54770, Punjab, Pakistan
[10]Phystech School of Aerospace Technology, Moscow Institute of Physics and Technology (MIPT), 9 Institutskiy Pereulok, Dolgoprudny, Moscow Region 141700, Russian Federation

DOI: https://doi.org/10.36348/sijcms.2026.v09i04.004 | **Received:** 28.05.2026 | **Accepted:** 21.07.2026 | **Published:** 25.07.2026

***Corresponding author:** Waheed Zaman Khan
Department of Physics, Division of Science and Technology, University of Education, College Road, Township, Lahore 54770, Punjab, Pakistan

Abstract

The transition toward carbon-neutral chemical manufacturing requires catalytic systems that can convert abundant waste molecules into value-added chemicals under mild, renewable-energy-driven conditions. Single-atom electrocatalysts (SAECs), featuring isolated metal centers anchored on tailored supports, offer maximum atom utilization, tunable coordination environments, and well-defined active sites for complex multielectron reactions. This review critically examines the emerging role of artificial intelligence in accelerating the discovery, optimization, and mechanistic understanding of SAECs for carbon dioxide electroreduction and green ammonia synthesis through nitrate conversion. First, fundamental design principles are discussed, including metal–support interactions, coordination engineering, electronic-structure modulation, and stability limitations. Next, machine learning, density functional theory integration, high-throughput screening, explainable descriptors, and self-driving laboratory concepts are evaluated as tools for rational catalyst development. Particular emphasis is placed on CO_2 valorization pathways toward CO, formate, hydrocarbons, and alcohols, together with nitrate-to-ammonia conversion as a sustainable nitrogen-recycling strategy. Advanced in situ/operando characterization, performance benchmarking, selectivity control, and degradation mechanisms are also assessed. Finally, this review highlights current barriers related to data quality, catalyst durability, reactor design, product separation, techno-economic feasibility, and industrial scale-up. The article provides a forward-looking framework for integrating AI, atomically precise catalysis, and renewable electrosynthesis in future sustainable chemical manufacturing.

Keywords: Artificial intelligence; Single-atom electrocatalysts; CO_2 electroreduction; Green ammonia synthesis; Nitrate reduction reaction; Carbon-neutral chemical manufacturing.

INTRODUCTION

Chemical manufacturing underpins fertilizers, polymers, pharmaceuticals, fuels, and numerous materials essential to modern society; however, its dependence on fossil carbon as both an energy source and feedstock creates a substantial climate burden. The sector accounts for approximately 5% of global CO_2 emissions and remains among the three largest industrial greenhouse-gas emitters, alongside steel and cement production (Gabrielli *et al*., 2023; Mallapragada *et al*., 2023). Emissions arise from fossil-fuel combustion for

process heat, electricity consumption, hydrogen production, and process-specific reactions, while carbon embedded in chemical products may be released at their end of life. Demand for major chemicals is nevertheless expected to continue growing, making efficiency improvements alone insufficient for deep decarbonization. Transitioning from thermochemical production powered by coal, oil, and natural gas toward renewable-electricity-driven synthesis is therefore strategically necessary. Electrification can replace fossil-derived heat, enable low-carbon hydrogen production through water electrolysis, and directly drive electrochemical transformations under comparatively mild temperatures and pressures (Eryazici *et al*., 2021; Mallapragada *et al*., 2023). Importantly, electrochemical manufacturing can couple renewable electrons with abundant or waste-derived feedstocks, including water, CO_2, and nitrate, thereby supporting both emission mitigation and circular resource use (Xia *et al*., 2022). Its climate benefit, however, depends strongly on electricity carbon intensity, conversion efficiency, product separation, catalyst durability, and full life-cycle impacts; electrification powered by carbon-intensive grids cannot automatically be classified as carbon neutral.A credible transition will consequently require coordinated expansion of renewable generation, flexible electrochemical reactors, energy-efficient separations, circular carbon management, and low-emission supply chains. Because renewable resources and industrial infrastructures vary geographically, no universal decarbonization pathway is sufficient. Integrated strategies combining electrification, recycling, sustainable feedstocks, carbon capture and utilization, and demand-side measures will be required to reconcile expanding chemical production with net-zero objectives (Gabrielli *et al*., 2023).

Electrocatalysis provides a direct interface between renewable electricity and chemical bond formation, allowing electrons to replace fossil-derived reductants and high-temperature process heat. In CO_2 electroreduction (CO_2RR), captured CO_2 can be converted into carbon monoxide, formate, methane, methanol, ethylene, ethanol, and other chemical building blocks. Product distribution is governed by catalyst identity, surface structure, electrolyte, local pH, mass transport, and applied potential because CO_2RR involves competing proton-coupled electron-transfer pathways and the hydrogen evolution reaction (Xia *et al*., 2022). Carbon monoxide and formate generally require fewer electron-transfer steps, whereas deeply reduced and C_2+ products demand multiple intermediates, carbon–carbon coupling, and stricter control of the reaction microenvironment. Consequently, renewable-powered CO_2RR could simultaneously valorize a greenhouse-gas feedstock and store intermittent electricity in chemical bonds, but its net climate benefit requires low-carbon power, durable electrodes, high single-pass conversion, and energy-efficient product separation.

Nitrate electroreduction offers a complementary route for circular nitrogen manufacturing. Nitrate accumulated through fertilizer runoff, industrial discharge, and wastewater treatment can be electrochemically converted to ammonia under comparatively mild conditions, linking pollution remediation with recovery of a valuable fertilizer and chemical feedstock (van Langevelde *et al*., 2021). Unlike direct N_2 reduction, nitrate reduction begins with a soluble, activated nitrogen oxyanion; nevertheless, the overall pathway involves sequential deoxygenation and hydrogenation through nitrite and adsorbed nitrogen-oxygen intermediates. Selective ammonia formation must therefore compete with nitrite accumulation, nitrogen-containing by-products, dinitrogen formation, and hydrogen evolution. Electricity source, nitrate concentration, electrolyte composition, reactor design, and ammonia recovery ultimately determine whether the process is environmentally and economically preferable to conventional removal and production routes.

At the level, electrochemical routes are modular and responsive to renewable generation, creating opportunities for production near carbon sources or nitrate-contaminated streams (Mallapragada *et al*., 2023). Their industrial relevance, however, depends on achieving meaningful current densities, selectivity, product concentration, energy efficiency, and operating lifetime rather than high Faradaic efficiency alone. Equally, carbon utilization does not guarantee carbon removal, because the lifetime and oxidation of products must be included in life-cycle accounting. These constraints make catalyst and reactor optimization inseparable from process-level assessment and renewable-energy integration.

Single-atom catalysts (SACs), in which isolated metal atoms are stabilized by defined coordination sites on solid supports, offer a compelling platform for controlling these multistep electrocatalytic reactions. Their atomic dispersion can approach complete utilization of the metal component, while metal identity, coordination number, neighboring heteroatoms, defects, and support interactions provide tunable electronic structures. These attributes can regulate adsorption energies and reaction pathways without requiring large quantities of scarce metals. For CO_2RR, computational screening has shown that stability, activity, and selectivity vary markedly across metal centers and coordination motifs, enabling identification of candidate sites before synthesis (Qi *et al*., 2022). For nitrate reduction, isolated sites may favor controlled intermediate binding and potentially suppress pathways requiring adjacent metal ensembles. However, SACs are not intrinsically superior: excessive intermediate binding, insufficient conductivity, low site density, metal leaching, and operando aggregation can negate theoretical advantages.

Artificial intelligence can accelerate exploration of this large design space by learning relationships among composition, coordination environment, electronic descriptors, adsorption energies, limiting potentials, and experimental performance. When trained on curated DFT or experimental datasets, supervised models, graph neural networks, and active-learning algorithms can rapidly rank candidates, reveal influential descriptors, and select informative calculations or experiments. For example, combined DFT–machine-learning workflows have screened hundreds of atomically dispersed structures and developed predictive structure–activity relationships for electrocatalysis (Chen *et al*., 2021; Qi *et al*., 2022). AI can also assist synthesis optimization, spectral interpretation, and closed-loop experimentation. Nevertheless, credible deployment requires uncertainty quantification, physically meaningful features, external validation, and protection against data leakage. Thus, AI should complement not replace electrochemical mechanism, operando characterization, and experimental verification.

Fundamentals of Single-Atom Electrocatalysts for Sustainable Chemistry

Structural Features of Single-Atom Catalysts

Single-atom catalysts (SACs) are heterogeneous materials in which individual metal atoms are spatially separated and anchored to a supporting matrix. Unlike nanoparticles, which contain surface and bulk atoms, an ideally dispersed SAC exposes nearly every metal atom to the reaction environment, enabling metal-utilization efficiencies approaching 100% in structurally uniform systems (Luo *et al*., 2023). This feature is particularly valuable for scarce metals such as Pt, Ir, Ru, and Pd. However, atomic dispersion alone does not define catalytic performance. The chemical identity of the isolated atom, its local coordination environment, oxidation state, electronic configuration, accessibility, and interaction with the support collectively determine whether it functions as an active, selective, and stable electrocatalytic site.

The coordination environment describes the number, chemical identity, and spatial arrangement of atoms directly bonded to the metal centre. Carbon-supported SACs commonly contain M–N_4, M–N_3, M–N_2, or mixed M–N_xC_γ configurations, whereas oxygen-, sulfur-, phosphorus-, and boron-containing ligands can create M–O, M–S, M–P, or M–B interactions. Conventional planar M–N_4 sites resemble metalloporphyrin motifs, but their electronic properties can be altered through coordination-number reduction, heteroatom substitution, axial ligation, lattice strain, or modification of neighboring carbon atoms (Song *et al*., 2023). For example, replacing nitrogen with less electronegative phosphorus changes electron redistribution around the metal centre and can substantially modify intermediate binding and reaction kinetics (Qian *et al*., 2024). Consequently, SACs with the same central metal may display different activities because their first and second coordination shells are not equivalent.

Metal–support interactions stabilize isolated atoms while simultaneously regulating their electronic structures. Charge transfer between the metal and support can change the metal oxidation state, d-orbital occupation, spin configuration, and position of frontier electronic states. These effects determine adsorption strength, activation barriers, and electron-transfer kinetics (Giulimondi *et al*., 2023). Strong covalent coordination can inhibit migration and aggregation, whereas overly strong binding may reduce structural flexibility or produce adsorption energies that are unfavorable for catalytic turnover. The support should therefore not be considered an inert carrier; it participates electronically and geometrically in constructing the active site. Metal oxides provide an especially clear illustration because oxygen vacancies, reducible cations, and lattice oxygen can modify charge localization and metal–support bonding (Han *et al*., 2024).

The atom-utilization advantage of SACs must also be interpreted cautiously. A high proportion of exposed metal does not guarantee a high density of electrochemically accessible sites, particularly when atoms are buried within carbon matrices or blocked by ionomers. Moreover, pyrolysis-derived materials often contain distributions of coordination motifs rather than a single uniform structure. Reliable structure–activity relationships therefore require complementary atomic-resolution microscopy, X-ray absorption spectroscopy, surface analysis, and theoretical modelling. SACs are best understood as coordination-defined, support-coupled active centres whose catalytic behavior emerges from the combined effects of atomic dispersion, local geometry, electronic structure, and the electrochemical microenvironment.

Table 1: Semi-quantitative comparison of common supports for single-atom electrocatalysts

Support material	Conductivity	Metal anchoring	Structural control	Stability	Scalability
Heteroatom-doped carbon	5	4	3	4	5
Graphene	5	3	4	3	3
Carbon nitride	2	5	4	3	4
MOFs	2	5	5	2	3
COFs	3	5	5	3	2
MXenes	5	4	4	2	3

Support material	Conductivity	Metal anchoring	Structural control	Stability	Scalability
Metal oxides	2	5	3	4	4
Defect-rich hybrid supports	4	5	3	4	2

Scoring scale: 1 = very low, 2 = low, 3 = moderate, 4 = high and 5 = very high. Scores represent comparative material-design tendencies rather than universal experimental values because performance depends on composition, synthesis, electrolyte and operating conditions.

Common Support Materials for Single-Atom Electrocatalysts

The support material performs three interconnected functions in SACs: it prevents metal-atom migration, establishes the coordination environment, and controls charge and mass transport. Carbonaceous supports—including activated carbon, carbon nanotubes, graphene, graphdiyne, carbon nanofibres, and porous carbon—are widely used because of their electrical conductivity, chemical tunability, surface area, and compatibility with scalable synthesis. Pristine graphitic carbon binds many metals weakly; consequently, vacancies, edges, micropores, and heteroatom dopants are introduced to create anchoring sites. Nitrogen-doped carbons are especially prominent because pyridinic, pyrrolic, and graphitic nitrogen can stabilize M–N_x motifs and redistribute charge within the carbon framework (Song *et al*., 2023). Co-doping with sulfur, phosphorus, boron, oxygen, or fluorine further tunes polarity, spin density, intermediate adsorption, and local hydrophilicity.

Graphene and related two-dimensional carbons offer rapid in-plane electron transport and structurally accessible surfaces. Nevertheless, restacking, limited intrinsic porosity, and weak binding on defect-free basal planes may restrict metal loading and accessibility. Defect engineering can address these limitations by creating carbon vacancies, topological defects, edges, and chemically unsaturated coordination pockets. Graphitic carbon nitride provides nitrogen-rich cavities capable of coordinating isolated metals without extensive external doping. Its heptazine- or triazine-based structure offers chemically defined anchoring environments, although modest conductivity, limited surface area, and structural alteration during thermal treatment can constrain electrocatalytic performance. Hybridization with conductive carbon is therefore frequently required.

Metal–organic frameworks (MOFs) and covalent organic frameworks (COFs) provide programmable pores and molecularly defined coordination sites. MOF metal nodes and organic linkers can directly host isolated atoms or serve as precursors for porous M–N–C materials after pyrolysis. Their ordered structures facilitate control of metal separation, but many pristine MOFs exhibit poor conductivity and limited electrochemical stability. Pyrolysis improves conductivity yet may destroy the original coordination precision and generate nanoparticles. COFs use covalent linkages and can incorporate bipyridine, porphyrin, phthalocyanine, or other chelating units to stabilize isolated metals at predetermined positions (Wu *et al*., 2024). Their structural designability and porosity are advantageous, although incomplete crystallinity, low conductivity, and linkage degradation remain practical concerns.

MXenes, typically represented as $M_{n+1}X_nT_x$, combine metallic conductivity with two-dimensional morphology and surface terminations such as –O, –OH, and –F. Vacancies and surface groups can anchor isolated metals and modify their electronic states, but MXene oxidation, sheet restacking, and instability under some potentials require careful control. Metal oxides—including TiO_2, CeO_2, FeO_x, CoO_x, and NiO—stabilize atoms through lattice oxygen, cation defects, and oxygen vacancies. Reducible oxides can mediate charge transfer and participate in catalytic cycles, although their conductivity may be lower than that of carbon supports (Han *et al*., 2024).

Other non-carbon supports include nitrides, carbides, sulfides, phosphides, hydroxides, and two-dimensional chalcogenides. These materials may contribute intrinsic catalytic functionality and form cooperative interfacial sites (Zheng *et al*., 2021). No support is universally optimal. Selection must balance binding strength, conductivity, porosity, corrosion resistance, metal loading, reactant accessibility, and compatibility with the intended potential, electrolyte, and reaction pathway.

Stability, Activity, and Selectivity Challenges in Atomically Dispersed Catalysts

The high surface free energy of isolated metal atoms creates an inherent tendency toward migration and aggregation. Although coordination to a support can kinetically stabilize atomic dispersion, electrochemical polarization, local heating, adsorbate binding, and support corrosion may weaken these interactions. Mobile atoms can combine into dimers, clusters, or nanoparticles through surface diffusion or dissolution–redeposition. Such transformations alter the number and identity of active sites and may either decrease performance or create a different catalyst from the one initially characterized. Accordingly, post-reaction evidence of isolated atoms cannot prove that the same structure remained active throughout operation; operando measurements are needed to establish the working state (Bae *et al*., 2023; Wang *et al*., 2025).

Metal leaching presents a related degradation route. Changes in potential and pH can modify metal oxidation state, dissolve weakly coordinated atoms, or

protonate anchoring heteroatoms. Carbon corrosion can remove coordination sites, while dissolution or reconstruction of oxide supports may release the metal centre. Coordination instability can also arise without complete metal loss: axial ligands may adsorb or desorb, M–N or M–O bonds may change, and the first coordination shell may be replaced by electrolyte-derived species. These processes can reversibly or irreversibly modify electronic structure. Dynamic reconstruction is therefore not always equivalent to deactivation, but it complicates assignment of intrinsic activity and demands characterization under realistic current density, electrolyte composition, and mass-transport conditions.

Activity optimization presents a second fundamental challenge. Isolated atoms must bind reactants strongly enough to activate them but weakly enough to release products, consistent with the Sabatier principle. Strong binding can poison the site with CO, nitrogen–oxygen species, or other intermediates, whereas weak binding produces poor surface coverage and high overpotential. Coordination engineering, axial ligation, defect regulation, and support-induced charge transfer can adjust adsorption energies; however, improvements predicted for one intermediate may strengthen another because adsorption energies often follow scaling relationships (Giulimondi *et al*., 2023). Low metal loading further limits geometric current density, whereas increasing loading reduces interatomic separation and promotes aggregation. Thus, maximizing atom utilization and maximizing practically available site density are distinct objectives (Luo *et al*., 2023).

Selectivity is particularly difficult in aqueous CO_2 and nitrate reduction because proton reduction to H_2 competes for electrons and surface sites. Suppressing the hydrogen evolution reaction requires appropriate intermediate binding, controlled proton delivery, and favorable local CO_2 or nitrate concentration. However, completely excluding adsorbed hydrogen may impede proton-coupled steps required for the desired product. Isolated sites can also be intrinsically unsuitable for pathways requiring neighboring atoms, including some carbon–carbon coupling reactions. Apparent selectivity therefore reflects the entire catalyst layer, electrolyte, ionomer, transport environment, and reactor not solely the nominal atomic site.

Long-term durability must be evaluated beyond short cycling tests. Meaningful assessment requires continuous operation, metal-loss quantification, product crossover analysis, post-test mass balance, and structural comparison before, during, and after catalysis. Stability should be reported at industrially relevant current densities rather than inferred from nearly unchanged polarization curves. Strategies such as vacancy confinement, strong coordination, spatial encapsulation, corrosion-resistant supports, and protective microenvironments can improve durability, but they must preserve accessibility. Ultimately, a practical SAC must maintain atomic identity, coordination structure, activity, and product selectivity simultaneously under sustained electrolysis.

AI-Guided Design, Screening, and Optimization of Single-Atom Electrocatalysts

Machine-Learning Models for Catalyst-Property Prediction

Machine learning (ML) provides a data-driven route for navigating the large compositional and configurational space of single-atom electrocatalysts (SACs). A typical SAC design space includes numerous metal centres, supports, coordination numbers, neighboring heteroatoms, defect structures, adsorbates, and reaction conditions. Evaluating every combination through experiments or density functional theory (DFT) is prohibitively expensive. ML models address this limitation by learning quantitative relationships between catalyst representations and target properties, thereby enabling rapid prescreening before computationally intensive calculations or synthesis.

Supervised-learning methods are most frequently used because catalyst datasets commonly contain labelled properties obtained from DFT or experiments. Linear and nonlinear regression predict continuous outputs such as adsorption energies, formation energies, limiting potentials, overpotentials, and Faradaic efficiencies. Classification algorithms can instead assign candidates to stability, activity, or selectivity classes. Random forests, gradient-boosting methods, support-vector machines, Gaussian-process regression, and artificial neural networks have all been applied to catalyst-property prediction. For example, extreme gradient-boosting regression successfully predicted intermediate-binding energies and limiting potentials for CO and formate production across SACs containing 3d–5d metals and different carbon–nitrogen coordination environments (Lin *et al*., 2024). Surrogate models can therefore replace a large fraction of repeated DFT calculations while retaining selected high-fidelity calculations for confirmation.

Model performance depends critically on catalyst representation. Physically meaningful descriptors may include metal electronegativity, ionization energy, atomic or covalent radius, valence-electron number, d-electron occupation, coordination number, support electronegativity, charge transfer, d-band centre, spin state, work function, and intermediate adsorption energy. Simple intrinsic descriptors are computationally inexpensive and interpretable, whereas electronic descriptors derived from DFT may provide stronger mechanistic resolution but reduce screening efficiency. Lin *et al.,*(2024) identified metal electronegativity–valence relationships, metal radius, and the average electronegativity of coordinating atoms as influential predictors of CO_2-reduction activity. Descriptor selection should nevertheless be performed

within cross-validation to prevent information leakage and artificially optimistic performance.

Deep-learning models can learn hierarchical representations directly from structural or electronic data, reducing dependence on manually selected descriptors. Graph neural networks (GNNs) are particularly suitable because catalysts can be represented as graphs in which atoms are nodes and interatomic connections are edges. Through message passing, a GNN learns how the chemical identity and local environment of neighboring atoms influence the target property. GAME-Net, for example, predicted molecular adsorption energies with a test mean absolute error of 0.18 eV and operated approximately six orders of magnitude faster than conventional DFT evaluation after training (Pablo-García *et al*., 2023). Similarly, adsorbate-environment graph models can rank surface configurations and direct additional DFT calculations toward the most informative structures (Ghanekar *et al*., 2022).

Adsorption energies remain central ML targets because they connect atomic structure with intermediate stabilization and reaction kinetics. DFT-derived free-energy diagrams identify the potential-determining step, from which the theoretical limiting potential can be calculated. ML models can predict these energies across large catalyst libraries and subsequently rank candidates by activity. Multi-output or classification models can compare competing pathways and anticipate product selectivity by evaluating the relative energetics of intermediates leading to CO, formate, methane, methanol, ammonia, hydrogen, or other products. Xi *et al.,* (2024), for example, combined high-throughput DFT with data-driven analysis to screen 192 transition-metal–TMD SACs and derive product-specific selection rules for CO_2 reduction.

Predictive accuracy alone is insufficient for credible catalyst discovery. Dataset imbalance, inconsistent DFT settings, narrow chemical coverage, correlated train–test splits, and extrapolation beyond the training domain can produce misleading results. Robust workflows require external testing, uncertainty quantification, interpretable feature analysis, and final DFT or experimental verification. ML should therefore function as an uncertainty-aware screening and hypothesis-generation tool rather than an independent substitute for physical modelling and electrocatalytic validation.

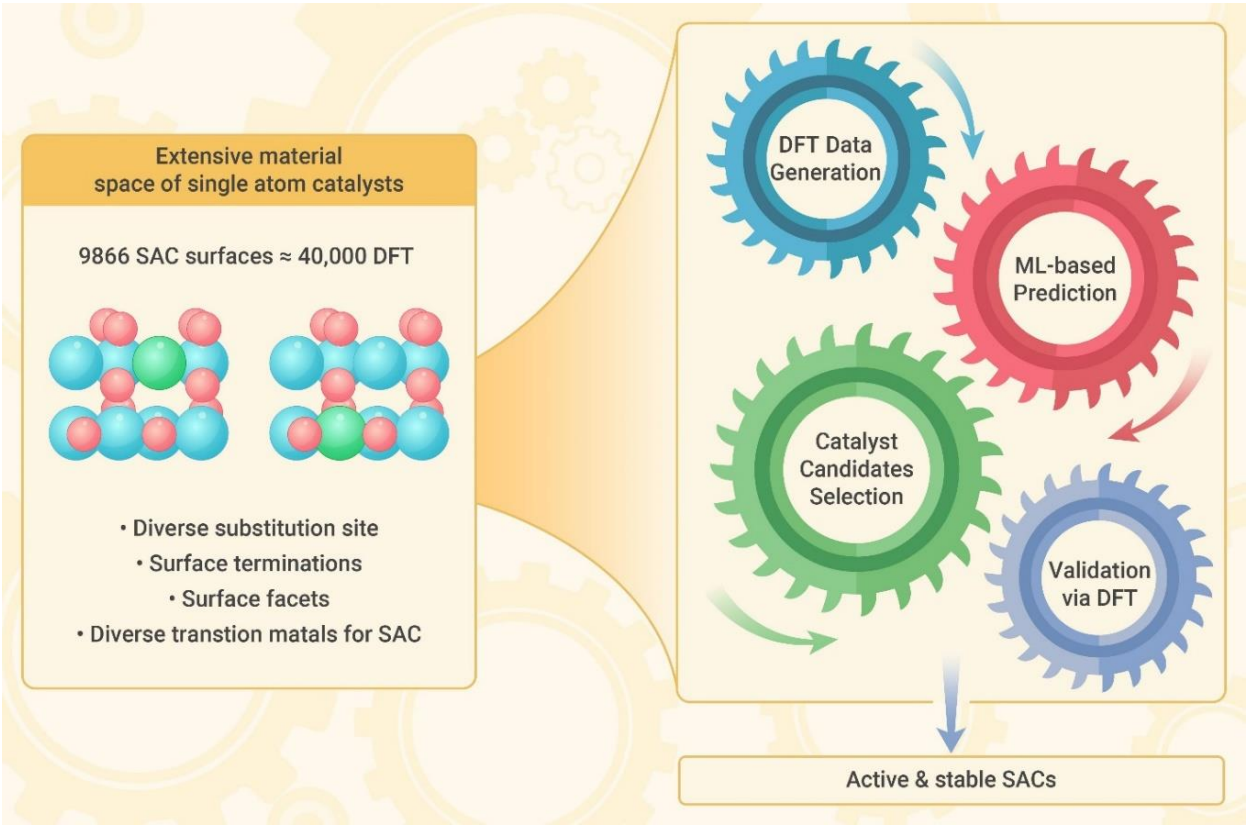

Figure 1: Integrated DFT–Machine-Learning Workflow for Property Prediction and High-Throughput Screening of Single-Atom Electrocatalysts

Figure 1. AI-assisted screening framework for single-atom electrocatalysts. A chemically defined candidate space is evaluated using selected DFT calculations, structural and electronic descriptors, supervised machine learning, uncertainty analysis, and activity–stability filters. High-ranking candidates are

subsequently returned for high-fidelity DFT and experimental validation. Adapted from Park *et al.,*(2024) under a CC BY licence.

DFT–AI Integration for High-Throughput Catalyst Discovery

The integration of DFT with machine learning provides a scalable strategy for converting quantum-mechanical calculations into predictive models that accelerate functional-material and catalyst discovery across large chemical spaces (Iqbal *et al*., 2025). Density functional theory provides atomistic data that connect SAC composition and coordination structure with thermodynamic stability, electronic properties, intermediate adsorption, and reaction energetics (Qi *et al*., 2022). In a DFT–AI workflow, representative metal–support structures are first calculated to establish a labelled dataset containing formation energies, dissolution potentials, adsorption energies, Gibbs free-energy changes, limiting potentials, and selectivity indicators (Lin *et al*., 2024). These data are transformed into descriptors describing metal identity, electronegativity, valence-electron configuration, atomic radius, coordination geometry, charge transfer, d-band position, support composition, and local defects (Tamtaji *et al*., 2023). Machine-learning models then approximate the DFT-derived structure–property relationship, allowing unevaluated candidates to be screened at substantially lower computational cost (Park *et al*., 2024).

For CO_2 reduction, DFT calculates the adsorption and conversion energetics of intermediates such as *COOH, *OCHO, *CO, *CHO, and *COH, which distinguish pathways toward CO, formate, methane, methanol, and other products (Lin *et al*., 2024). The largest positive free-energy step determines the theoretical limiting potential, while comparison with hydrogen adsorption provides an initial selectivity criterion against the hydrogen evolution reaction (Qi *et al*., 2022). Regression models can learn adsorption energies or limiting potentials, whereas classification models can assign candidates to product-selectivity or activity classes (Lin *et al*., 2024). High-throughput screening of 192 transition-metal–TMD SACs demonstrated that calculated free-energy profiles could be combined with data-driven analysis to derive product-specific design rules for CO_2 electroreduction (Xi *et al*., 2024). Such models reduce the candidate space before more rigorous constant-potential calculations, microkinetic modelling, or experimental validation are performed (Xi *et al*., 2024).

The same strategy can accelerate nitrate-to-ammonia catalyst discovery, although NO_3RR involves a more complex sequence of adsorption, deoxygenation, and hydrogenation steps (Ding *et al*., 2024). Relevant labels include SAC formation energy, nitrate adsorption energy, free energies of $*NO_3$, $*NO_2$, *NO, *NHO, *NH, and $*NH_2$, and the limiting potential for ammonia formation (Lu *et al*., 2025). Selectivity filters should additionally compare ammonia formation with nitrite release, N_2 formation, and competitive hydrogen evolution (Lu *et al*., 2025). Lu *et al.,* (2025) trained ML models using calculated stability, adsorption, and reaction-energy information and predicted the performance of 1,891 previously unexamined SACs. A four-stage screening process based on stability, nitrate adsorption, activity, and selectivity identified ten candidates, two of which were subsequently examined through additional calculations (Lu *et al*., 2025). In a separate metalloporphyrin study, DFT and interpretable ML identified NbPP, TaPP, and WPP as promising NO_3RR catalysts with calculated limiting potentials of −0.24, −0.28, and −0.33 V, respectively (Ding *et al*., 2024).

The reliability of DFT–AI screening depends on consistent computational settings and chemically representative datasets (Lin *et al*., 2024). Mixing energies obtained with incompatible functionals, solvation models, reference states, or electrode-potential treatments introduces systematic errors that ML may reproduce rather than correct (Pablo-García *et al*., 2023). Random train–test splitting can also overestimate transferability when closely related coordination structures occur in both subsets (Pablo-García *et al*., 2023). Robust workflows therefore require chemically separated validation, uncertainty estimation, domain-of-applicability analysis, and targeted recalculation of uncertain candidates (Park *et al*., 2024). Predicted catalysts must ultimately be tested experimentally because simplified DFT models may omit explicit electrolyte structure, potential-dependent reconstruction, mass transport, and kinetic barriers (Lu *et al*., 2025).

Table 2: Quantitative examples of DFT–machine-learning screening for atomically dispersed electrocatalysts

Target reaction	Initial computational space	Screening output	Quantitative result	Source
CO_2RR on TM@TMD SACs	192 structures	3 leading candidates	Fe@CoS_2, Pt@$TiTe_2$ and Co@CoS_2 selected for HCOOH, CH_4 and CH_3OH pathways	Xi *et al.,* (2024)
NO_3RR on diverse SACs	1,891 predicted structures	10 candidates; 2 computationally revalidated	Four filters: stability, NO_3^- adsorption, activity and selectivity	Lu *et al.,* (2025)

Target reaction	Initial computational space	Screening output	Quantitative result	Source
NO_3RR on metalloporphyrins	Metalloporphyrin SAC library	3 leading candidates	Calculated limiting potentials: NbPP, −0.24 V; TaPP, −0.28 V; WPP, −0.33 V	Ding *et al.,* (2024)
OER on oxide-supported SACs	795 binary supports combined with 21 metals	14 candidates	ML reduced binding-energy evaluation cost by more than tenfold	Park *et al.,* (2024)

Abbreviations: CO_2RR, carbon dioxide reduction reaction; NO_3RR, nitrate reduction reaction; OER, oxygen evolution reaction; SAC, single-atom catalyst; TM, transition metal; TMD, transition-metal dichalcogenide.

Self-Driving Laboratories and Closed-Loop Catalyst Optimization

Self-driving laboratories integrate automated experimentation, robotics, real-time characterization, data management, and algorithmic decision-making within an iterative closed loop (Tom *et al*., 2024). Unlike conventional high-throughput experimentation, which executes a predetermined sequence, a closed-loop system analyzes completed measurements and autonomously chooses the next experiment according to a defined objective (Tom *et al*., 2024). For SAC discovery, this loop could connect precursor selection, support functionalization, synthesis conditions, electrochemical testing, product analysis, and structural characterization to an active-learning controller (Jenewein *et al*., 2024). The objective may involve maximizing Faradaic efficiency and current density while simultaneously minimizing overpotential, precious-metal content, and degradation (Jenewein *et al*., 2024).

Automated synthesis requires machine-addressable control of precursor concentration, pH, temperature, mixing, deposition, pyrolysis, washing, and electrode fabrication (Tom *et al*., 2024). Liquid-handling robots can prepare compositional libraries, while automated furnaces, flow reactors, and deposition systems can vary thermal or chemical parameters reproducibly (Tom *et al*., 2024). Robotic electrochemical workstations can subsequently conduct polarization, impedance, selectivity, and stability measurements using standardized protocols (Jenewein *et al*., 2024). Integration with chromatography, mass spectrometry, spectroscopy, and computer vision enables rapid extraction of product and catalyst information (Tom *et al*., 2024). However, autonomous decisions are only trustworthy when calibration, blanks, contamination controls, metadata capture, and failure detection are incorporated into the workflow (Tom *et al*., 2024).

Active learning selects experiments that are expected to improve a predictive model most efficiently, often by balancing uncertain regions against candidates predicted to perform well (Jenewein *et al*., 2024). Bayesian optimization is especially useful when experiments are expensive and only a small number of observations are initially available (Shields *et al*., 2021). A probabilistic surrogate model estimates both the expected response and its uncertainty, while an acquisition function recommends the next experimental conditions (Shields *et al*., 2021). Expected improvement, upper-confidence bound, probability of improvement, and entropy-based criteria provide different balances between exploitation and exploration (Shields *et al*., 2021). Multiobjective Bayesian optimization can identify a Pareto front rather than collapsing competing requirements into a single arbitrary score (Bennett *et al*., 2024).

The practical capability of autonomous experimentation has already been demonstrated in catalytic and chemical systems (Burger *et al*., 2020). A mobile robotic chemist completed 688 photocatalysis experiments over eight days and identified a hydrogen-evolution formulation approximately six times more active than the initial conditions (Burger *et al*., 2020). An automation–Bayesian-optimization platform achieved conversions above 80% for four substrates after 23 experiments, sampling approximately 0.2% of the defined combinatorial space (Schilter *et al*., 2024). Multiobjective optimization has also been applied to non-noble acidic oxygen-evolution electrocatalysts, illustrating its relevance to catalyst spaces governed by activity, stability, and composition simultaneously (Jenewein *et al*., 2024).

Transferring this capability to SACs remains challenging because atomic dispersion and coordination structure are more difficult to measure automatically than bulk composition (Tom *et al*., 2024). A nominal synthesis recipe may produce isolated atoms, clusters, nanoparticles, or mixtures, making structural verification essential before performance data are returned to the algorithm (Tom *et al*., 2024). Operando X-ray absorption and microscopy are not yet readily available in routine robotic loops, while accelerated electrochemical tests may fail to predict long-term durability (Tom *et al*., 2024). Near-term platforms should therefore operate with human supervision, explicit uncertainty limits, standardized data schemas, and periodic high-fidelity characterization (Tom *et al*., 2024). The credible objective is not a completely unsupervised laboratory, but an auditable closed-loop system in which automation increases reproducibility and AI directs experiments while researchers retain control over mechanistic interpretation and validation (Tom *et al*., 2024).

AI-Guided Single-Atom Electrocatalysts for CO_2 Conversion

Reaction Pathways and Product Selectivity in CO_2 Electroreduction

Electrochemical CO_2 reduction involves coupled electron-transfer, proton-transfer, adsorption, and bond-forming steps that can generate products ranging from two-electron C_1 compounds to deeply reduced C_2+ chemicals (Chen *et al*., 2024). The product distribution depends on the catalyst, applied potential, electrolyte, local pH, interfacial electric field, surface coverage, and availability of protons and CO_2 near the active site (Birdja *et al*., 2021). Hydrogen evolution competes for electrons and surface sites throughout the process, making selective intermediate stabilization essential (Chen *et al*., 2024).

Formation of CO commonly proceeds through initial CO_2 activation and proton-coupled electron transfer to adsorbed *COOH, followed by water elimination to form *CO (Birdja *et al*., 2021). Weak-to-moderate *CO binding permits CO desorption, which explains the high CO selectivity of many Fe-, Co-, Ni-, Zn-, Ag-, and Au-centred catalysts (Chen *et al*., 2024). Formate follows a different branch involving oxygen-bound *OCHO, which is subsequently protonated and released as $HCOO^-$ or HCOOH (Dong *et al*., 2023). Sn-, Bi-, In-, and selected Cu-based sites generally favour this pathway because their electronic structures stabilize *OCHO relative to *COOH (Dong *et al*., 2023).

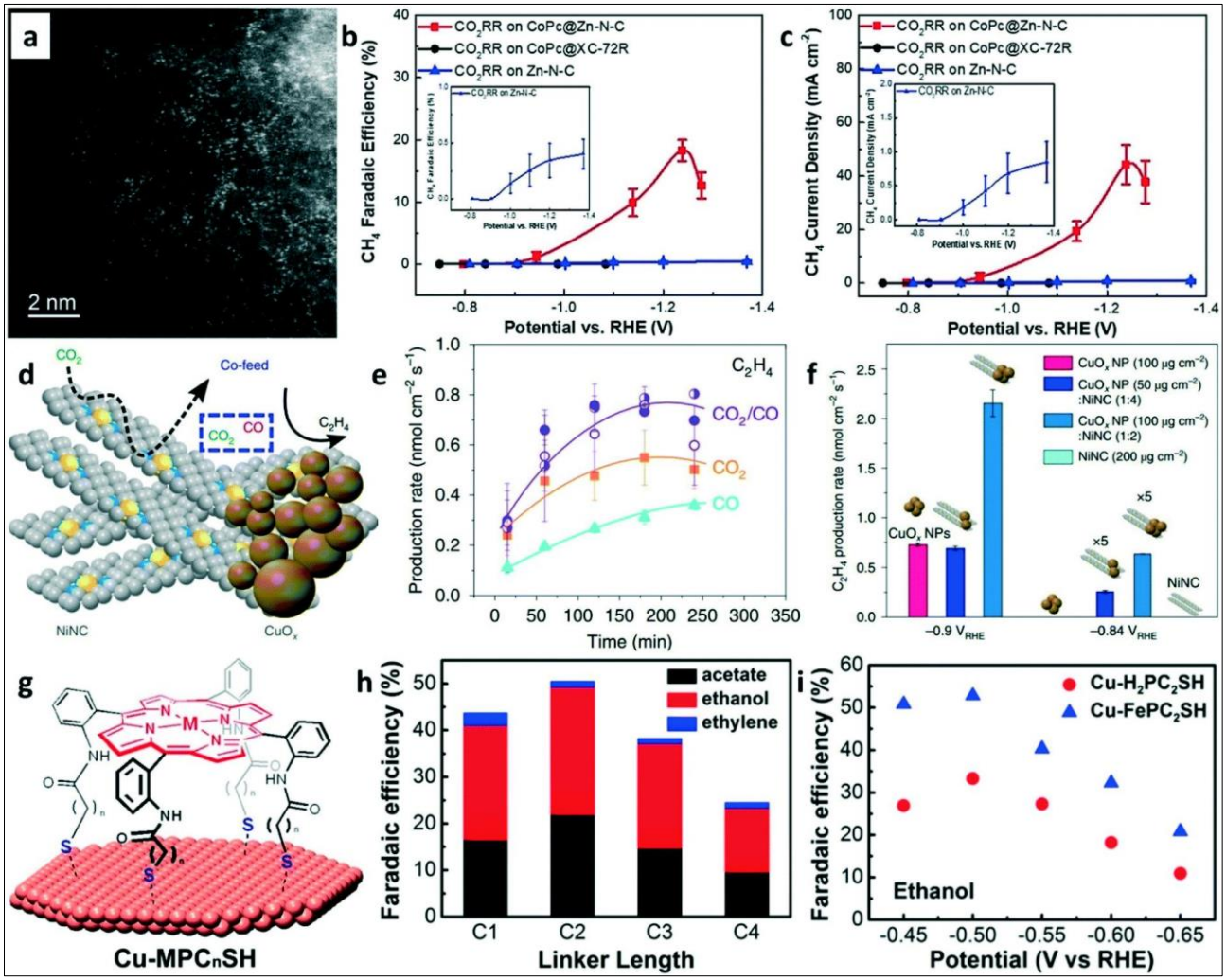

Figure 2: Reaction Network Governing C_1 and C_2+ Product Selectivity During Electrochemical CO_2 Reduction

Methanol and methane require deeper reduction beyond *CO and therefore involve multiple proton–electron transfers (Nitopi *et al*., 2021). Adsorbed *CO may be hydrogenated through *CHO or *COH, followed by intermediates such as *CHOH, $*CH_2O$, $*CH_2OH$, and $*CH_3O$ (Nitopi *et al*., 2021). Branching between oxygen retention and C–O bond cleavage influences whether methanol or methane is formed (Chen *et al*., 2024). Methane production generally requires efficient C–O cleavage and sequential hydrogenation, whereas methanol requires retention of the oxygen functionality until product desorption (Nitopi *et al*., 2021). Isolated Zn sites have been reported to redirect CO_2 reduction from CO toward methane by altering the energetics of

multielectron intermediates, demonstrating that single atoms are not necessarily restricted to two-electron products (Han *et al*., 2020).

Ethylene, ethanol, acetate, and other C_2+ products require carbon–carbon bond formation (Nitopi *et al*., 2021). On copper surfaces, C–C coupling is commonly associated with *CO dimerization or coupling between *CO and a hydrogenated carbon intermediate (Nitopi *et al*., 2021). Subsequent protonation, oxygen removal, and hydrogenation determine whether the coupled intermediate produces ethylene, ethanol, or another oxygenate (Birdja *et al*., 2021). A strictly isolated single atom may be geometrically unable to bind two carbon intermediates simultaneously; consequently, C_2+ formation often requires adjacent atoms, paired atomic sites, support-assisted coupling, tandem configurations, or potential-induced restructuring (Chen *et al*., 2024). Reports of multicarbon production over nominal SACs therefore require operando verification to exclude aggregation into clusters or nanoparticles (Martini *et al*., 2023).

Product selectivity cannot be attributed to adsorption energy alone because mass transport and reactor architecture alter local reactant and intermediate concentrations (Birdja *et al*., 2021). Gas-diffusion electrodes and membrane-electrode assemblies can overcome aqueous CO_2-solubility limitations, but carbonate formation and flooding may reduce carbon efficiency (Chen *et al*., 2024). Reliable pathway assignment therefore requires product mass balance, isotope-labelled CO_2 controls, operando spectroscopy, potential-dependent characterization, and comparison with hydrogen evolution under identical conditions (Martini *et al*., 2023).

Figure 2. Principal reaction pathways for electrochemical CO_2 conversion on atomically dispersed metal sites. Initial proton-coupled electron transfer produces either *COOH or *OCHO, directing selectivity toward CO or formate, respectively. Further hydrogenation of *CO generates methanol* or methane, whereas coupling between adjacent carbon-containing intermediates enables ethylene, ethanol, and other C_2+ products. Adapted from Chen *et al.,* (2024) under a CC BY 3.0 licence.

4.2. Single-Atom Active Sites for CO_2 Reduction

M–N–C materials constitute the most extensively studied SAC family for CO_2 electroreduction because nitrogen ligands stabilize isolated metals and regulate their charge, orbital occupation, and intermediate-binding strength (Pan *et al*., 2023). Although M–N_4 is the conventional motif, experimentally relevant structures also include M–N_2, M–N_3, M–N_5, mixed M–N/C/O/S coordination, axial ligands, and defect-associated sites (Pan *et al*., 2023). Coordination number, symmetry, and second-shell chemistry can therefore produce substantially different performance for the same metal (Dong *et al*., 2023).

Fe–N–C catalysts commonly favour CO formation through stabilization of *COOH followed by sufficiently facile *CO desorption (Chen *et al*., 2024). Altering Fe coordination number or adding axial oxygen can redistribute electron density and improve the balance between CO_2 activation and CO release (Pan *et al*., 2023). Co–N_x sites similarly favour CO, but coordination-specific studies demonstrate that Co–N_4 may provide substantially higher selectivity than undercoordinated Co–N_2 or Co–N_3 structures (Zhang *et al*., 2024). Ni–N–C catalysts are among the most selective CO-producing SACs because low-valent Ni sites can activate CO_2 while binding CO weakly enough to avoid poisoning (Chen *et al*., 2024). A square-pyramidal Ni–N_5–C catalyst achieved CO Faradaic efficiency exceeding 97% across a broad potential range and reached 99.6% at a current density of 1.23 A cm^{-2} (Huang *et al*., 2022).

Cu SACs exhibit more diverse behaviour because Cu can support CO, formate, methane, and, under particular configurations, multicarbon formation (Dong *et al*., 2023). Planar-symmetry-broken CuN_3 produced formate with 94.3% selectivity at −0.73 V versus RHE, compared with 72.4% for a symmetric CuN_4 reference at −0.93 V (Dong *et al*., 2023). The CuN_3 catalyst retained more than 90% formate selectivity at an average current density of 94.4 mA cm^{-2} for 100 h, demonstrating the importance of local geometric distortion (Dong *et al*., 2023). However, Cu atoms may migrate or aggregate under reducing potentials, so C_2+ production must be interpreted alongside operando structural evidence (Martini *et al*., 2023).

Zn–N–C generally supports CO production, although suitable microporous coordination environments can facilitate methane formation (Han *et al*., 2020). A Zn SAC achieved approximately 85% methane Faradaic efficiency, a methane partial current density of −31.8 mA cm^{-2}, and 35 h stability, illustrating coordination-dependent access to deeper reduction pathways (Han *et al*., 2020). Sn and Bi centres preferentially stabilize oxygen-bound *OCHO and are therefore primarily associated with formate production (Deng *et al*., 2023). Operando spectroscopy has shown that axial oxygen coordination can modify isolated Sn sites during CO_2 electrolysis, emphasizing that the active structure may differ from its ex situ form (Deng *et al*., 2023). Bi single atoms anchored on carbon have produced formic acid with a reported Faradaic efficiency of 83.6%, although activity and stability remain sensitive to loading and support structure (Zhang *et al*., 2024).

Metal–support effects extend beyond mechanical stabilization (Chen *et al*., 2024). Charge transfer, vacancies, axial ligands, local hydrophobicity,

pore confinement, and neighboring heteroatoms modify CO_2 adsorption, proton accessibility, and intermediate energetics (Pan *et al*., 2023). Consequently, meaningful comparisons require active-site density, metal loading, current density, electrolyte, cell architecture, potential reference, carbon efficiency, and stability to be reported together rather than ranking catalysts by peak Faradaic efficiency alone (Chen *et al*., 2024).

Table 3: Quantitative performance of representative single-atom catalysts for CO_2 electroreduction

Catalyst/site	Principal product	Maximum FE	Reported operating condition	Durability	Source
Ni–N_5–C	CO	99.6%	1.23 A cm^{-2} at −2.4 V vs. RHE	100 h	Huang *et al.,* (2022)
PSB-CuN_3	Formate	94.3%	−0.73 V vs. RHE	>90% selectivity for 100 h at 94.4 mA cm^{-2}	Dong *et al.,* (2023)
Symmetric CuN_4	Formate	72.4%	−0.93 V vs. RHE	Reference catalyst	Dong *et al.,* (2023)
Zn single atoms on N-doped carbon	CH_4	85%	−31.8 mA cm^{-2} CH_4 partial current at −1.8 V vs. SCE	35 h	Han *et al.,* (2020)
Bi single atoms/carbon	HCOOH	83.6%	Carbon-supported Bi atomic sites	Not directly comparable	Zhang *et al.,* (2024)
Er SAC	CO	≥90%	Up to 500 mA cm^{-2} in neutral and acidic media	100 h at 100 mA cm^{-2}	Wang *et al.,* (2025)

FE, Faradaic efficiency; RHE, reversible hydrogen electrode; SCE, saturated calomel electrode. Values should not be ranked directly because electrolyte, cell configuration, catalyst loading, potential and product-analysis procedures differ among studies.

AI-Assisted Prediction of CO_2-Reduction Performance

AI-assisted catalyst design converts structural, elemental, electronic, and experimental information into models that predict CO_2RR stability, activity, and selectivity before extensive synthesis (Lin *et al*., 2024). A typical workflow begins with a curated DFT or experimental dataset, represents each catalyst using descriptors, trains regression or classification models, evaluates uncertainty, and validates high-ranking predictions using new calculations or experiments (Park *et al*., 2024). For SACs, relevant inputs include metal electronegativity, ionization energy, atomic radius, valence-electron number, d-electron occupation, coordination number, ligand electronegativity, metal–ligand distance, charge transfer, spin state, and intermediate adsorption energies (Lin *et al*., 2024).

Adsorption energies of *COOH, *OCHO, *CO, and *H are particularly useful because they approximate CO_2 activation, product branching, CO release, and competition with hydrogen evolution (Qi *et al*., 2022). These quantities can be converted into free-energy diagrams and limiting potentials for CO or formate production (Lin *et al*., 2024). Extreme-gradient-boosting models have predicted binding energies and limiting potentials across 3d–5d metal centres and eight carbon–nitrogen coordination environments (Lin *et al*., 2024). Feature analysis identified combinations of metal electronegativity, valence-electron number, atomic radius, and coordinating-atom electronegativity as influential descriptors (Lin *et al*., 2024). Such interpretable variables are preferable to purely statistical correlations because they can suggest experimentally actionable modifications.

Graph neural networks provide an alternative when manually engineered descriptors cannot capture complex local environments (Pablo-García *et al*., 2023). By treating atoms as nodes and chemical connections as edges, graph models learn how coordination geometry and neighboring atoms affect adsorption or reaction energies (Pablo-García *et al*., 2023). Nevertheless, their improved flexibility requires larger datasets and rigorous validation against structures outside the training distribution (Pablo-García *et al*., 2023). Physics-informed models can reduce this risk by incorporating adsorption-energy relationships, charge conservation, thermodynamic constraints, or reaction-network structure (Chen *et al*., 2025).

Experimental Faradaic efficiency is more difficult to predict than DFT adsorption energy because it depends on catalyst structure, potential, electrolyte, reactor architecture, mass transport, catalyst loading, and product quantification (Raman *et al*., 2025). Stacked ML models have nevertheless been developed to predict CO Faradaic efficiency from experimental and catalyst variables, demonstrating the potential for data-guided operating-condition selection (Raman *et al*., 2025). Such predictions must be accompanied by uncertainty intervals because literature datasets contain inconsistent reporting and relatively few negative results (Raman *et al*., 2025). Random splitting may also place nearly identical catalysts in both training and test sets,

producing inflated performance estimates (Chen *et al*., 2025).

AI can reduce trial-and-error synthesis by ranking candidate metals, coordination motifs, supports, and operating conditions before laboratory preparation (Song *et al*., 2025). Inverse-design frameworks extend this concept by generating structures optimized for multiple objectives rather than merely predicting known candidates (Song *et al*., 2025). One generative AI workflow created more than 250,000 candidate alloy structures, increased the proportion of predicted high-activity structures by 2.5-fold relative to random generation, and experimentally validated five candidates, two of which delivered approximately 90% CO_2RR Faradaic efficiency (Song *et al*., 2025). Although this example involved alloys rather than SACs, the closed design–prediction–validation principle is directly transferable to atomically dispersed catalysts.

For Q-category research, AI-predicted SACs should be treated as hypotheses until validated through standardized electrochemistry and operando characterization (Martini *et al*., 2023). High-confidence discovery requires transparent datasets, chemically separated testing, uncertainty-aware acquisition, consistent DFT settings, and experimental confirmation of atomic dispersion under working conditions (Martini *et al*., 2023). AI is therefore most valuable as a mechanism-linked decision tool that narrows the search space while preserving physical interpretation and experimental accountability.

AI-Guided Single-Atom Electrocatalysts for Green Ammonia Synthesis

Nitrate-to-Ammonia Conversion as a Sustainable Nitrogen Pathway

Nitrate contamination originates primarily from fertilizer runoff, livestock waste, industrial effluents and incomplete nitrogen removal during wastewater treatment, contributing to eutrophication and deterioration of drinking-water quality (van Langevelde *et al*., 2021). Conventional nitrate-removal technologies, including ion exchange, reverse osmosis, biological denitrification and electrodialysis, often transfer nitrate into a concentrated waste stream or convert reactive nitrogen into N_2 rather than recovering it as a useful product (Chen *et al*., 2024). Electrocatalytic nitrate reduction to ammonia (NO_3RR) offers a different strategy by combining water remediation, nitrogen recovery and chemical production within one electricity-driven process (Gao *et al*., 2022).

The overall acidic reaction involves eight electrons and nine protons:

$$NO_3^- + 9H^+ + 8e^- \rightarrow NH_3 + 3H_2O$$

although the actual proton donor and dominant nitrogen species depend on electrolyte pH (Wu *et al*., 2021). Nitrate is initially adsorbed or protonated and then sequentially deoxygenated through nitrite and nitrogen–oxygen intermediates, which may include *NO_3, *NO_2, *NO, *NHO, *NOH and *NH_2OH (Wu *et al*., 2021). Subsequent hydrogenation produces *N, *NH, *NH_2 and *NH_3 before ammonia desorption (Niu *et al*., 2021). Because this pathway involves numerous proton- and electron-transfer events, the catalyst must balance nitrate adsorption, N–O bond cleavage, hydrogen supply and ammonia release (Zhang *et al*., 2024).

NO_3RR is kinetically more accessible than direct electrochemical N_2 reduction because nitrate is soluble in water and does not require initial cleavage of the exceptionally stable N≡N bond (van Langevelde *et al*., 2021). It can also operate near ambient temperature and pressure using renewable electricity, providing a potential route for distributed ammonia production close to nitrate-containing water sources (Wu *et al*., 2021). Nevertheless, nitrate-derived ammonia should not automatically be described as carbon neutral because electricity generation, electrolyte preparation, reactor construction, ammonia separation and nitrate-source concentration affect its overall environmental burden (Huang *et al*., 2024). The process is most compelling when it treats an existing waste stream while recovering concentrated ammonia with limited downstream energy demand (Gao *et al*., 2022).

Reaction selectivity remains a central challenge because nitrate can form nitrite, nitric oxide, nitrous oxide, hydroxylamine, N_2 or ammonia (Zhang *et al*., 2024). Hydrogen evolution competes for electrons and surface hydrogen, particularly at negative potentials, while insufficient proton supply may cause nitrite accumulation in alkaline electrolytes (Liao *et al*., 2024). Conversely, excessive hydrogen coverage can block nitrate adsorption and decrease nitrogen utilization (Zhang *et al*., 2024). Catalyst composition, surface structure, nitrate concentration, pH, cations, applied potential and hydrodynamics therefore jointly control the reaction pathway (Halder *et al*., 2025).

Practical implementation requires coupling electrosynthesis with ammonia recovery because dilute NH_3 solutions have limited commercial value and may create secondary pollution if discharged (Farghali *et al*., 2024). Membrane separation, gas stripping, electrodialysis and conversion into ammonium salts are potential recovery routes, but each adds energy and material requirements (Farghali *et al*., 2024). Performance should consequently be evaluated using nitrate conversion, ammonia selectivity, Faradaic efficiency, yield rate, energy consumption, product concentration, nitrogen mass balance and stability in authentic wastewater (Huang *et al*., 2024). This system-level assessment distinguishes meaningful nitrogen recycling from high laboratory selectivity obtained in concentrated, purified nitrate electrolytes.

Single-Atom Catalysts for the Nitrate Reduction Reaction

Single-atom catalysts provide isolated, electronically tunable metal centres capable of controlling nitrate adsorption and the sequential transformation of nitrogen–oxygen intermediates (Subhadarshini *et al*., 2024). Carbon-supported M–N–C structures are particularly attractive because nitrogen ligands stabilize individual transition-metal atoms while modifying their oxidation state, spin configuration and binding strength toward $*NO_3$, $*NO_2$ and *NO (Wu *et al*., 2021). The most common configuration is $M–N_4$, although $M–N_2$, $M–N_3$, $M–N_5$, mixed M–N/O/S coordination and single-atom alloys can exhibit substantially different reaction energetics (Subhadarshini *et al*., 2024).

$Fe–N_4$ is among the best-characterized NO_3RR active sites. Wu *et al.,* (2021) reported an Fe SAC with an ammonia Faradaic efficiency of approximately 75% and a yield rate approaching 20,000 μg h^{-1} mg_cat^{-1}. DFT identified *NO reduction to *HNO and subsequent *HNO conversion to *N as potential-limiting steps, with a calculated limiting potential of −0.30 V versus RHE (Wu *et al*., 2021). The absence of adjacent Fe atoms made N–N coupling energetically unfavorable, suppressing N_2 and N_2O formation and directing adsorbed nitrogen toward ammonia (Wu *et al*., 2021). Metal-normalized ammonia production was approximately 20 times higher for Fe SACs than for the corresponding Fe nanoparticle catalyst (Wu *et al*., 2021).

Cu-based atomic catalysts are effective because Cu can adsorb nitrate and facilitate its initial deoxygenation while maintaining comparatively limited hydrogen evolution (Zhang *et al*., 2024). However, Cu alone may release nitrite or bind later intermediates inadequately, motivating the introduction of isolated secondary metals (Cai *et al*., 2022). A Ni single-atom alloy on Cu reached approximately 100% ammonia Faradaic efficiency and a yield rate of 326.7 μmol h^{-1} cm^{-2} at −0.55 V versus RHE (Cai *et al*., 2022). The isolated Ni atom strengthened interaction with the crucial *NOOH intermediate, lowered the limiting potential and inhibited by-product formation (Cai *et al*., 2022). Similarly, an Au/Cu single-atom alloy achieved 99.69% ammonia Faradaic efficiency at −0.80 V versus RHE, demonstrating the value of isolated promoters within conductive metal hosts (Gao *et al*., 2023).

Co, Ni, Ru, Ag, Zn and other atomic centres have also been explored, although their performance depends strongly on coordination and electrolyte conditions (Subhadarshini *et al*., 2024). $Fe–N_4$ was calculated to have a lower limiting potential than analogous $Co–N_4$ and $Ni–N_4$ sites, illustrating that changing only the central metal can alter the rate-limiting hydrogenation step (Wu *et al*., 2021). Noble-metal atoms such as Ru may promote N–O cleavage and hydrogenation but require high atom utilization and stable anchoring to justify their cost (Subhadarshini *et al*., 2024). Ag atomic sites can provide high ammonia selectivity by moderating hydrogen adsorption, although activity at dilute nitrate concentration remains a critical consideration (Yin *et al*., 2025).

Coordination engineering offers a route to balance adsorption and hydrogenation. Reducing coordination number, introducing axial oxygen, replacing nitrogen with sulfur or phosphorus, and modifying second-shell dopants can change charge localization and intermediate-binding strength (Subhadarshini *et al*., 2024). Strong nitrate binding alone is insufficient because the site must also promote N–O cleavage without becoming poisoned by *NO or *N (Niu *et al*., 2021). Excessively favourable hydrogen adsorption accelerates HER, whereas insufficient surface hydrogen slows the conversion of *NO-derived intermediates to ammonia (Zhang *et al*., 2024). Practical SAC design must therefore optimize nitrate capture, intermediate conversion, proton delivery, ammonia desorption and resistance to aggregation simultaneously.

Table 4: Quantitative performance of representative atomic-site catalysts for nitrate-to-ammonia conversion

Catalyst	Atomic-site structure	NH_3 FE	NH_3 yield rate	Potential	Mechanistic contribution	Source
Fe SAC	$Fe–N_4$/NC	≈75%	≈20,000 μg h^{-1} mg_cat^{-1}; 0.46 mmol h^{-1} cm^{-2}	Maximum-performance region reported in the original study	Suppresses N–N coupling and favours sequential hydrogenation	Wu *et al.,* (2021)
Ni_1Cu single-atom alloy	Isolated Ni in Cu host	≈100%	326.7 μmol h^{-1} cm^{-2}	−0.55 V vs. RHE	Stabilizes *NOOH and suppresses by-products	Cai *et al.,* (2022)
Au_1Cu single-atom alloy	Isolated Au in Cu host	99.69%	See original study for normalization	−0.80 V vs. RHE	Regulates nitrate activation and hydrogenation on Cu	Gao *et al.,* (2023)
Fe/Cu diatomic catalyst	Adjacent Fe–Cu sites	92.51%	1.08 mmol h^{-1} mg^{-1} at −0.50 V	−0.30 V vs. RHE for maximum FE	Fe promotes nitrate adsorption; Cu assists electron transfer	Zhang *et al.,* (2023)

Ru single atoms/Co–NC	Ru–N_x on Co–NC	96.3%	1.12 mmol h^{-1} cm^{-2}	−0.50 V vs. RHE	Enhances N–O cleavage and intermediate hydrogenation	Guo *et al.,* (2025)

FE, Faradaic efficiency; NC, nitrogen-doped carbon; RHE, reversible hydrogen electrode. Direct ranking is inappropriate because nitrate concentration, electrolyte, reactor configuration, catalyst loading and yield normalization differ among studies.

Machine-Learning and Mechanistic Modelling for Ammonia Selectivity

The large number of possible metals, supports, coordination environments and reaction intermediates makes NO_3RR well suited to DFT-assisted machine learning (Lu *et al*., 2025). A conventional computational workflow calculates formation energy, nitrate adsorption, reaction free energies and hydrogen adsorption for a representative SAC dataset (Ding *et al*., 2024). These labels are combined with descriptors such as metal electronegativity, atomic radius, valence-electron configuration, coordination number, metal–ligand distance, charge transfer and d-band position to train regression or classification models (Lu *et al*., 2025). The resulting model rapidly evaluates candidates that have not undergone explicit DFT calculations.

Catalyst screening should proceed through sequential physical filters rather than a single activity score (Lu *et al*., 2025). Formation or binding energy can first exclude unstable metal–support combinations, after which nitrate adsorption removes sites unable to capture NO_3^- (Lu *et al*., 2025). Limiting potential and free energy of the potential-determining step are then used to assess ammonia activity, while comparison with hydrogen evolution and competing nitrogen products provides a selectivity filter (Ding *et al*., 2024). Lu *et al.,* (2025) applied this strategy to predict the performance of 1,891 previously unexamined SACs and identified ten candidates after stability, adsorption, activity and selectivity screening. Two leading candidates were subsequently re-evaluated computationally, illustrating the appropriate use of ML as a prescreening rather than final-validation tool (Lu *et al*., 2025).

Mechanistic modelling must capture intermediates beyond initial nitrate adsorption because ammonia formation involves eight electrons and multiple surface configurations (Wu *et al*., 2021). DFT free-energy diagrams identify potential-limiting transformations, whereas transition-state calculations and microkinetic models estimate reaction rates and surface coverage (Niu *et al*., 2021). On Fe–N_4, *NO reduction and subsequent *HNO transformation were identified as key energetic steps, while nitrite was experimentally confirmed as a reaction intermediate (Wu *et al*., 2021). A descriptor based only on nitrate adsorption would therefore miss the kinetic importance of downstream nitrogen–oxygen hydrogenation.

Interpretable machine learning can reveal structure–activity relationships by ranking descriptors and identifying nonlinear interactions (Ding *et al*., 2024). In metalloporphyrin SACs, charge on the transition-metal centre, coordination characteristics and metal–nitrogen distances influenced nitrate adsorption and predicted NO_3RR performance (Ding *et al*., 2024). NbPP, TaPP and WPP were identified as promising candidates with calculated limiting potentials of −0.24, −0.28 and −0.33 V, respectively (Ding *et al*., 2024). More recent interpretable modelling has emphasized that local doping patterns, coordination geometry and intermediate structure can outperform elemental properties alone as predictors of ammonia activity (Zhu *et al*., 2026).

AI models may eventually predict experimental Faradaic efficiency, but this target is more complex than a DFT-derived limiting potential (Lu *et al*., 2025). Faradaic efficiency depends on nitrate concentration, electrolyte pH, applied potential, catalyst loading, proton transport, reactor hydrodynamics and analytical recovery of nitrogen products (Huang *et al*., 2024). Literature datasets frequently mix different normalization conventions and omit complete nitrogen balances, limiting model transferability (Huang *et al*., 2024). Models trained on such data may learn laboratory-specific correlations instead of intrinsic catalytic behaviour.

Reliable AI-guided discovery therefore requires standardized DFT settings, chemically separated train–test sets, uncertainty quantification and experimental validation using isotope-labelled nitrate when contamination is possible (Lu *et al*., 2025). Predicted sites must also be characterized under operating conditions because potential-driven changes in oxidation state or aggregation can invalidate the assumed atomic model (Subhadarshini *et al*., 2024). The strongest approach integrates interpretable ML, DFT, microkinetics, operando spectroscopy and nitrogen mass balance to connect atomic structure with experimentally verified ammonia selectivity.

Figure 5. DFT-derived minimum-energy pathway for nitrate-to-ammonia conversion on an Fe–N_4 single-atom catalyst. Sequential deoxygenation and hydrogenation proceed through adsorbed nitrogen–oxygen and nitrogen–hydrogen intermediates. The free-energy profiles at 0.00 V and the calculated limiting potential of −0.30 V versus RHE identify *NO-to-HNO and subsequent hydrogenation as critical energetic steps. Adapted from Wu *et al.,* (2021) under the article's open-access licence.

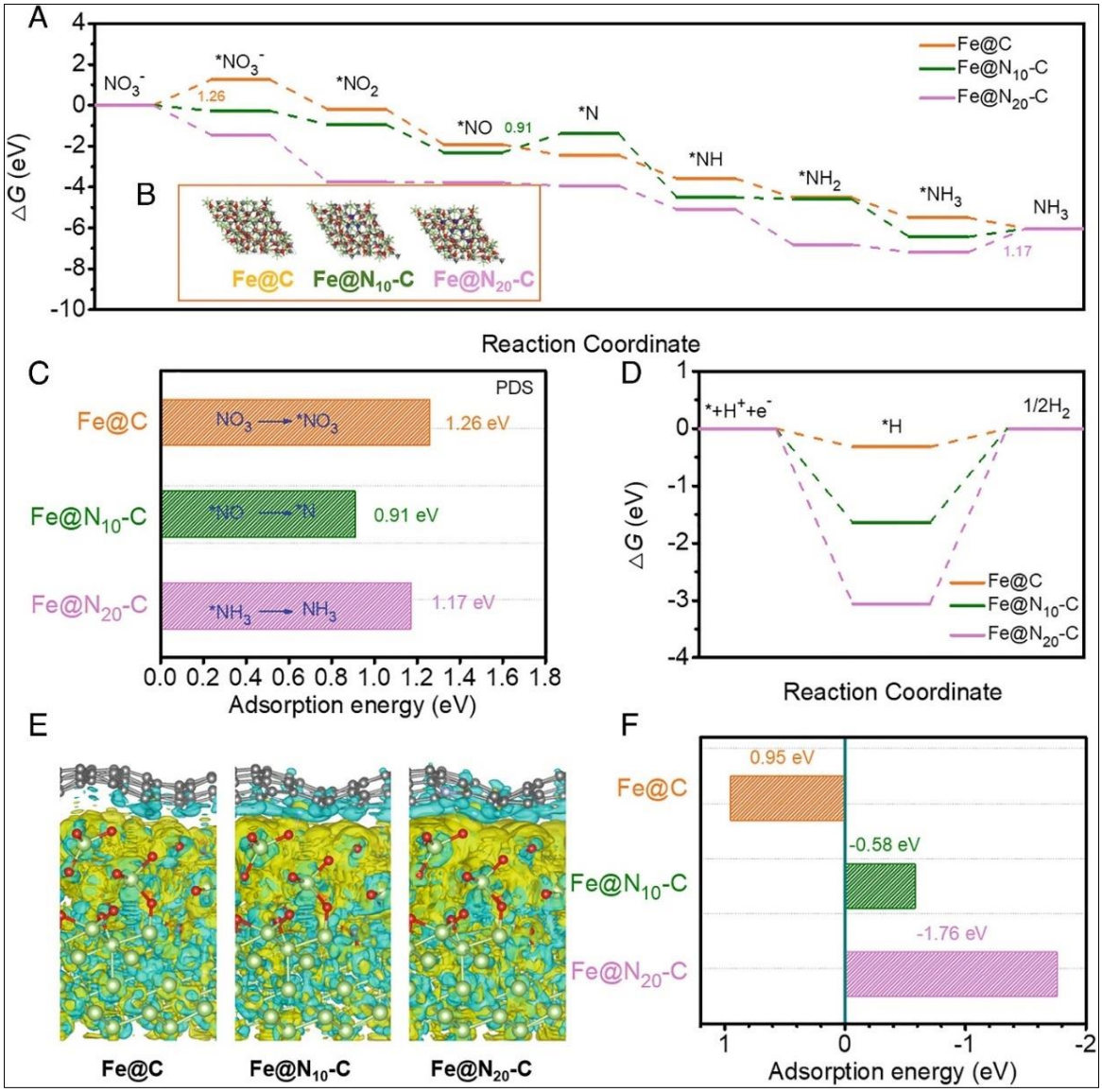

Figure 3: Minimum-Energy Pathway and Potential-Dependent Free-Energy Profile for Nitrate-to-Ammonia Conversion on an Fe–N_4 Single-Atom Site

Characterization, Mechanistic Understanding, and Performance Evaluation

Advanced Characterization of Single-Atom Active Sites

Reliable identification of single-atom electrocatalysts (SACs) requires convergent evidence because no individual technique can simultaneously establish atomic dispersion, coordination geometry, oxidation state, and operando stability. High-angle annular dark-field scanning transmission electron microscopy (HAADF-STEM) provides the most direct spatial evidence of isolated atoms. Its approximate atomic-number-dependent contrast makes heavy metal atoms appear as bright spots on lighter supports. However, a limited field of view, beam-induced migration, overlap with support atoms, and difficulty imaging low-atomic-number metals prevent HAADF-STEM from proving that every metal atom is isolated. Representative images should therefore be complemented by statistically meaningful analysis of multiple regions and bulk-sensitive spectroscopy (Kottwitz *et al*., 2021; Qi *et al*., 2022).

X-ray absorption spectroscopy (XAS) is particularly valuable because it is element-specific, compatible with dilute catalysts, and applicable under reaction conditions. X-ray absorption near-edge structure (XANES) probes oxidation state, orbital occupancy, and coordination symmetry through edge position, white-line intensity, and pre-edge features. Extended X-ray absorption fine structure (EXAFS) provides average coordination numbers, absorber–scatterer distances, and structural disorder. A dominant first-shell M–N or M–O contribution accompanied by no detectable M–M scattering supports atomic dispersion. Nevertheless, the absence of an EXAFS M–M shell is not

definitive evidence of exclusively isolated atoms because minority clusters may remain below the technique's detection limit. Model-dependent fitting, parameter correlations, and ensemble averaging must also be acknowledged (Finzel *et al*., 2023). Wavelet-transform EXAFS can strengthen scatterer discrimination but does not remove these fundamental limitations.

X-ray photoelectron spectroscopy (XPS) identifies surface composition, metal oxidation states, and support functionalities. Shifts in metal, N 1s, O 1s, or C 1s binding energies can reveal charge transfer and candidate M–N_x configurations. However, peak assignments are rarely unique, while air exposure, charging, and ex situ relaxation may produce states different from those operating electrochemically (Kottwitz *et al*., 2021). Raman spectroscopy complements XPS by assessing carbon defects through the D- and G-band response and detecting catalyst-induced changes in support disorder. Infrared spectroscopy, particularly attenuated-total-reflection surface-enhanced FTIR, can identify metal–ligand vibrations and adsorbed species such as *CO, *COOH, *NO_x, and *NH_x.

For Fe-containing SACs, ^57Fe Mössbauer spectroscopy offers unusually specific information on oxidation state, spin configuration, coordination symmetry, and the relative abundance of Fe species. Its operando implementation can distinguish reversible electronic changes from irreversible demetallation or aggregation, although isotope enrichment, long acquisition times, and specialized facilities may be required (Zeng *et al*., 2021). Consequently, rigorous SAC characterization should integrate microscopy, XAS, XPS, vibrational spectroscopy, elemental analysis, and operando measurements. Such triangulation separates three distinct claims: isolated atoms are present, their average coordination structure is identified, and that structure remains catalytically relevant under working conditions.

Table 6: Evidence hierarchy and analytical limitations of techniques used to characterize single-atom electrocatalysts

Technique	Primary quantitative observable	SAC information obtained	Important limitation
HAADF-STEM	Atomic-position intensity and interatomic distribution	Direct visualization of spatially isolated atoms	Local sampling; beam damage; weak contrast for light metals
XANES	Edge energy, white-line intensity, pre-edge response	Oxidation state, electronic configuration, coordination symmetry	Reference- and model-dependent interpretation
EXAFS	Coordination number, bond distance, Debye–Waller factor	Average M–N/O/C environment and possible M–M coordination	Minority clusters may remain below detection limits
XPS	Binding energy and surface atomic concentration	Surface oxidation state, charge transfer, ligand chemistry	Ex situ alteration and ambiguous peak deconvolution
Raman	D/G-band ratio, band position and width	Defect density and metal–support perturbation	Indirect evidence of metal coordination
FTIR	Vibrational frequency and potential-dependent intensity	Adsorbates and reaction intermediates at or near active sites	Band overlap and water absorption
Mössbauer	Isomer shift, quadrupole splitting, magnetic field	Fe/Sn oxidation, spin state, symmetry, and species fractions	Restricted isotopes and relatively long acquisition
Operando XAS	Time- and potential-dependent XANES/EXAFS	Working-state reconstruction and electronic dynamics	Ensemble averaging and demanding cell design

Operando and In Situ Mechanistic Studies

Ex situ characterization describes a catalyst before or after electrolysis, but it cannot establish the identity of the active state because applied potential, electrolyte, adsorbates, and local pH can reversibly or irreversibly transform single-atom sites. *In situ* measurements examine catalysts within a controlled reaction environment, whereas *operando* experiments simultaneously record structural or spectroscopic information and catalytic performance. This distinction is important: structural evolution becomes mechanistically meaningful only when synchronized with current and product formation.

Operando XAS is among the most powerful approaches for following SAC evolution. Potential-dependent XANES edge shifts reveal changes in average oxidation state, while EXAFS identifies changes in coordination number, bond length, and possible M–M scattering. Martini *et al.,* (2023) combined operando XAS with supervised and unsupervised machine learning to deconvolute coexisting metal environments in transition-metal–nitrogen–carbon catalysts during CO_2 electroreduction. The work demonstrated that nominally similar M–N–C materials can contain multiple site populations and that their concentrations evolve under polarization. Such findings caution against assigning activity exclusively to a single ex situ M–N_4 model.

Vibrational methods provide complementary molecular information. Operando attenuated-total-reflection FTIR and surface-enhanced infrared absorption spectroscopy can follow potential-dependent *COOH and *CO during CO_2 reduction and nitrate-derived *NO_2, *NO, *NHO, and *NH_x species during nitrate reduction. Isotopic experiments using ^$13CO_2$ or ^$15NO_3^-$ strengthen assignments because predictable frequency shifts distinguish genuine reaction intermediates from electrolyte impurities or support-derived signals. Raman spectroscopy can detect changes in support bonding, surface oxides, metal–ligand coordination, and interfacial carbonate species. Nevertheless, spectral assignments should be supported by isotope labeling, density-functional-theory-calculated frequencies, and potential-response reversibility rather than relying on band position alone.

Active-site reconstruction can involve ligand protonation, axial adsorption, coordination-number changes, migration, dissolution, or conversion from isolated atoms into clusters. Conversely, clusters can redisperse into atomically coordinated species. Operando electron microscopy offers spatially resolved evidence of migration, but realistic liquid electrochemical environments and electron-beam effects remain challenging. Online inductively coupled plasma mass spectrometry can detect metal dissolution, while differential electrochemical mass spectrometry and online gas chromatography correlate gaseous products with structural transitions. Product sampling must be temporally matched to spectroscopy; otherwise, rapid intermediates may be compared with time-averaged product distributions.

Mechanistic verification therefore requires an integrated time axis. A credible assignment should demonstrate that a spectroscopic species emerges within the catalytic potential window, tracks a product-specific partial current, responds reversibly to potential changes, and agrees with isotopic and theoretical evidence. Even these correlations do not automatically establish causality because spectators can follow the same potential dependence as active intermediates. Perturbation experiments potential steps, reactant switching, isotopic exchange, controlled poisoning, and modulation-excitation spectroscopy provide stronger kinetic discrimination. Operando evidence should ultimately replace static "structure–activity" descriptions with working-state structure–intermediate–rate relationships, which are substantially more useful for AI training and rational SAC design (Martini *et al*., 2023; Wang *et al*., 2025).

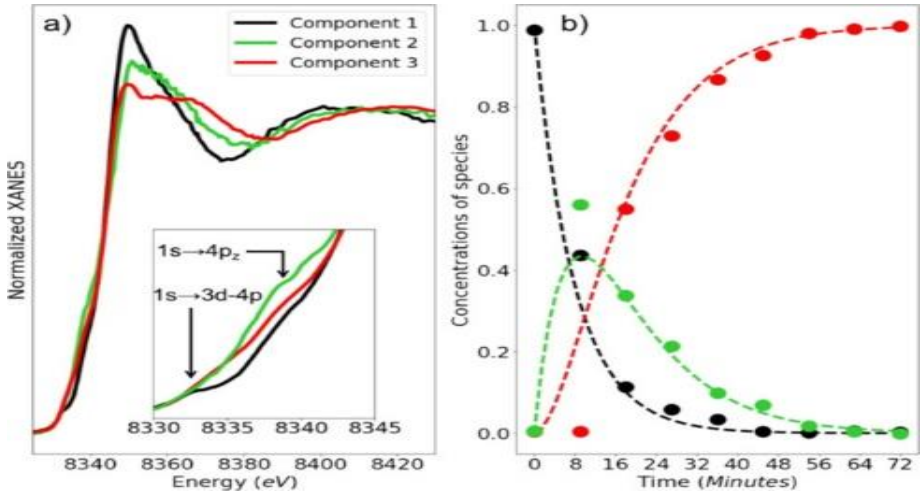

Figure 4: Operando identification of dynamically evolving Ni sites in a Ni–N–C single-atom catalyst during CO_2 electroreduction

Ni K-edge XANES spectra of three pure spectral components extracted from operando measurements, including an expanded pre-edge region that reflects differences in the electronic and coordination structures of the Ni centers. (b) Time-dependent concentrations of the three components obtained by target-transformation analysis. The dashed curves represent fitting with a consecutive first-order transformation model, demonstrating the disappearance of the initial Ni species, transient formation of an intermediate, and accumulation of a final working-state species. Subsequent machine-learning-assisted XANES simulations were used to assign plausible atomistic structures to these components. Reproduced from Martini *et al.,* (2023) under the Creative Commons Attribution 4.0 International License.

Standard Performance Metrics and Reliability Assessment

Performance comparisons between SAC electrocatalysts are meaningful only when activity, selectivity, productivity, energy demand, and durability are reported under sufficiently similar conditions. Current density describes the reaction rate per geometric electrode area, but total current includes all electrochemical processes. Product-specific partial

current density, calculated as total current density multiplied by the product Faradaic efficiency (FE), is therefore more informative. Both geometric and catalyst-mass-normalized values should be reported, together with catalyst loading, electrochemically active area where defensible, uncompensated resistance correction, electrolyte composition, temperature, pressure, and reactor configuration (Seger *et al*., 2023).

FE quantifies the fraction of charge producing a particular product. It must be calculated from measured product quantities, electron stoichiometry, and total charge rather than inferred from current alone. For gaseous products, calibrated flow rates and gas-chromatographic concentrations are required; dissolved products require calibrated NMR, ion chromatography, colorimetry, or other validated analyses. Product crossover, volatilization, carbonate formation, incomplete phase sampling, corrosion, and unreported liquid volume changes can produce erroneous carbon or nitrogen balances. The sum of product FEs should approach 100%, and unexplained deficits or values exceeding 100% must be investigated (Kempler & Nielander, 2023).

Turnover frequency (TOF) is attractive for SACs because atomically dispersed metals appear countable; however, dividing product rate by total metal loading assumes that every metal atom is accessible and catalytically equivalent. This assumption is rarely demonstrated. Authors should state whether TOF uses total metal atoms, electrochemically accessible sites, or a site density measured by chemisorption, stripping, or probe reactions. Accordingly, many published TOFs should be described as apparent or lower-bound values. Yield rate should be expressed with explicit normalization—such as mmol NH_3 h^{-1} cm^{-2}, mmol h^{-1} mg_cat^{-1}, or mol product h^{-1}—and accompanied by FE and current density.

Energy efficiency should combine voltage efficiency and Faradaic selectivity using the thermodynamic cell potential and the measured full-cell voltage. Reporting cathode potential alone omits anode losses, membrane resistance, and balance-of-plant penalties. For industrial relevance, full-cell energy consumption, product concentration, single-pass conversion, carbon or nitrogen utilization, and separation requirements are more informative than half-cell performance. CO_2 electrolysis additionally requires carbon balances because carbonate crossover may create apparently high selectivity while lowering net CO_2 utilization (Ma *et al*., 2020; Seger *et al*., 2023).

Stability testing should report continuous operating time, potential or current drift, product-specific FE, product concentration, and post-test metal loss. Constant current without repeated product analysis cannot prove selective stability. At least three independently prepared electrodes should be evaluated, with error bars representing biological or preferably catalyst-batchreplicates rather than repeated measurements of one electrode. Benchmarking should use identical reactors, loadings, electrolytes, flow rates, potentials, and analytical protocols. Raw calibration curves, chromatograms, spectra, metal loadings, and uncertainty propagation should be available. For nitrate reduction, $^{15}NO_3^-$ controls and blank tests are particularly important for excluding ambient ammonia contamination. Reliable reporting thus treats performance as a multidimensional dataset rather than a record FE or current-density value.

Table 7: Minimum quantitative reporting framework for SAC electrocatalysis

Metric	Recommended unit or expression	Essential accompanying information
Total current density	mA cm^{-2}_geo	Electrode area, iR correction, loading and reactor
Product partial current	j_product = j_total × FE_product	Product identity and electron stoichiometry
Faradaic efficiency	%	Calibration, sampling interval, charge and phase balance
TOF	s^{-1} or h^{-1}	Definition and measurement of active-site population
Yield rate	mmol h^{-1} cm^{-2} or mmol h^{-1} mg_cat^{-1}	Catalyst loading, electrolyte volume and duration
Energy efficiency	% or kWh $kg\_product^{-1}$	Full-cell voltage, FE, thermodynamic basis
Selectivity	FE and product distribution	All detectable products and mass balance
Stability	Hours at specified j or potential	Time-dependent FE, voltage, concentration and metal loss
Reproducibility	Mean ± SD, n ≥ 3	Independent catalyst batches/electrodes
Benchmarking	Matched-condition comparison	Same cell, electrolyte, loading and analytical method

Challenges, Industrial Translation, and Future Perspectives

Scientific and Technical Barriers to Practical Application

Despite rapid advances in single-atom electrocatalysts (SACs), translation from laboratory activity to continuous chemical manufacturing remains constrained by coupled catalyst, electrode, reactor, and separation challenges. The first concern is degradation of

atomically dispersed sites. Because isolated atoms possess high surface free energy, applied potential, adsorbate coverage, local pH, and Joule heating can trigger metal migration, agglomeration, dissolution, or coordination-shell reconstruction. Carbon corrosion and demetallation further destabilize M–N–C catalysts, while strongly adsorbed *CO, *NO_x, sulfur species, or electrolyte impurities may poison accessible sites. Consequently, stable current alone cannot demonstrate catalyst durability; time-resolved product selectivity, metal dissolution, full-cell voltage, and operando coordination measurements are required (Nwabara *et al*., 2020; Belsa *et al*., 2024).

CO_2 electrolysis presents additional electrode-level instability. Gas-diffusion electrodes can undergo flooding, salt precipitation, carbonate accumulation, ionomer redistribution, hydrophobicity loss, and membrane crossover. These phenomena alter the three-phase interface and frequently cause selectivity to shift toward hydrogen evolution. Industrial deployment assessments identify operation above approximately 1 A cm^{-2} and durability approaching five years as important system-level objectives, far beyond the tens or hundreds of hours commonly demonstrated in laboratory devices (Guerra *et al*., 2023). Accelerated durability protocols incorporating potential cycling, impurity exposure, start–stop operation, electrolyte-concentration changes, and cumulative-charge testing are therefore needed, but they must reproduce realistic degradation mechanisms rather than merely accelerate failure (Nwabara *et al*., 2020).

Product dilution constitutes a second major barrier. CO_2 reduction generates gaseous products mixed with unreacted CO_2 or dilute oxygenates in catholyte streams. Nitrate reduction may produce ammonia in a large electrolyte volume, particularly when environmentally relevant nitrate concentrations are used. High Faradaic efficiency at low reactant conversion does not guarantee a separation-ready product stream. Product concentration, single-pass conversion, carbon or nitrogen utilization, water transport, and recovery energy must therefore accompany catalyst-level metrics.

Mechanistic complexity also limits rational scale-up. CO_2 reduction involves parallel proton- and electron-transfer pathways, surface-bound intermediates, local alkalization, and carbon–carbon coupling. Nitrate-to-ammonia conversion requires eight-electron transfer and can generate nitrite, nitric oxide, hydroxylamine, nitrogen, or hydrogen. Conditions that optimize one elementary step may inhibit another, and SACs may reconstruct into clusters or adsorbate-coordinated sites under operating conditions.

Finally, increasing electrode area introduces nonuniform pressure, temperature, reactant concentration, current distribution, and catalyst loading. Performance measured on a small electrode cannot be extrapolated linearly to a stack. Translation therefore requires manufacturable catalyst deposition, uniform gas and liquid distribution, low-resistance membranes, impurity tolerance, modular stack design, automated control, and operando diagnosis under technically relevant conditions (Bagemihl *et al*., 2023; Guerra *et al*., 2023).

Table 8: Quantitative translation benchmarks and present validation requirements

Translation parameter	Suggested system-level objective	Required supporting measurement
CO_2-electrolyzer current density	>1 A cm^{-2}	Product-specific partial currents and area uniformity
Full-cell voltage	<3 V for low-temperature CO_2 electrolysis	Cathode, anode, membrane and ohmic-loss contributions
Commercial durability aspiration	>5 years	Degradation rate, selectivity retention and stack availability
Laboratory durability reporting	Continuous, product-verified operation	FE, product concentration and voltage versus time
Nitrate-reduction selectivity	Preferably >90% FE_NH_3	^15NO_3^- verification and complete nitrogen balance
Reproducibility	≥3 independent electrodes or batches	Mean, standard deviation and failure distribution
Product recovery	Report concentration and single-pass conversion	Separation energy and recycle requirements
Material retention	Before/after metal inventory	ICP-MS dissolution and operando/post-mortem structure

The >1 A cm^{-2}, <3 V and >5-year CO_2-electrolysis objectives are system-development benchmarks discussed by Guerra *et al.,* (2023), rather than universal catalyst acceptance thresholds.

Techno-Economic and Environmental Assessment

Techno-economic assessment (TEA) and life-cycle assessment (LCA) are essential because high

catalytic activity does not necessarily produce an economically competitive or environmentally beneficial process. The cost of electrochemical manufacturing is determined by electricity consumption, stack capital cost, catalyst and membrane replacement, reactant preparation, product recovery, compression, recycling, capacity factor, and plant lifetime. Multiscale analysis has shown that current density, cell voltage, conversion, selectivity, mass transport, and reactor dimensions are interdependent; treating them as independent optimistic parameters can underestimate production costs (Bagemihl *et al*., 2023).

Electricity is commonly the dominant operating input. Lowering cathodic overpotential is beneficial, but industrial energy consumption depends on full-cell voltage, including the anodic reaction, membrane resistance, contact losses, pumps, and downstream processing. Pairing CO_2 or nitrate reduction with a lower-energy anodic oxidation could reduce cell voltage and generate a second product, although the availability, price, and purification of the anodic feedstock must be included. Intermittent renewable electricity further introduces start–stop cycling, partial-load operation, storage requirements, and capacity-factor penalties. A catalyst optimized only at steady current may therefore perform poorly in a wind- or solar-coupled plant (Guerra *et al*., 2023).

Product separation can overturn apparent catalyst-level advantages. Gaseous CO or syngas may be separated from residual CO_2 through pressure-swing adsorption or related operations, whereas dilute formate, alcohols, or ammonia may require evaporation, distillation, membrane separation, absorption, or crystallization. Separation energy increases sharply as product concentration decreases. Accordingly, TEA should use measured outlet concentration, single-pass conversion, crossover, and recycle composition instead of Faradaic efficiency alone. Carbonate formation in alkaline CO_2 electrolysis also consumes CO_2 and electrolyte and can impose regeneration costs (Belsa *et al*., 2024).

SACs may reduce catalyst cost by maximizing metal utilization, particularly for scarce metals. Nevertheless, atom efficiency does not automatically imply low cost. Precursors, ligands, high-temperature pyrolysis, acid leaching, inert gases, low batch yield, quality control, and specialized supports may dominate manufacturing expense. Industrial evaluation should therefore report metal loading, synthesis yield, energy consumption, solvent use, catalyst recovery, electrode-coating rate, and replacement frequency. Earth-abundant Fe, Co, Ni or Cu sites are attractive, but environmental burdens from mining and catalyst loss remain relevant.

LCA must define the electricity mix, CO_2 source, nitrate source, system boundary, coproduct allocation, catalyst lifetime, and displaced conventional process. CO_2 conversion is not intrinsically carbon neutral: fossil-intensive electricity or short-lived carbon products can eliminate the climate advantage. Nitrate-to-ammonia conversion offers the combined value of nitrogen recovery and water remediation, but its benefit depends on nitrate concentration, avoided treatment, electricity carbon intensity, and ammonia recovery. Prospective LCA should consequently be coupled with TEA and uncertainty analysis. Industrial feasibility is most credible when experimentally measured stack performance is propagated through material and energy balances, rather than when isolated record metrics are inserted into idealized process models.

Table 9: Minimum inputs for integrated TEA–LCA of SAC-based electrochemical manufacturing

Category	Required quantitative inputs	Principal outcome affected
Electricity	Full-cell voltage, current, capacity factor, electricity price and carbon intensity	Operating cost and climate impact
Electrolyzer	Current density, area, stack cost, lifetime and replacement rate	Capital cost and availability
Selectivity	Product FE and competing-product distribution	Feed utilization and purification load
Conversion	Single-pass conversion and recycle ratio	Reactor and compressor sizing
Product stream	Concentration, phase and flow rate	Separation energy and equipment
Catalyst	Loading, synthesis yield, precursor cost and metal loss	Catalyst cost and resource burden
Feedstock	CO_2 capture cost or nitrate concentration and pretreatment	Delivered reactant cost
Environmental boundary	Electricity mix, CO_2 origin, avoided treatment and coproduct allocation	Life-cycle greenhouse-gas result

Future Outlook: Explainable AI, Digital Catalysis, and Autonomous Carbon-Neutral Manufacturing

The next phase of AI-guided SAC development should move beyond black-box performance prediction toward interpretable, uncertainty-aware models connected to experimentally accessible chemistry. Explainable AI can identify whether predicted activity originates from coordination number, metal electronegativity, d-electron configuration, support defects, adsorption energetics, or electrolyte conditions. Feature-attribution methods, symbolic regression, physically constrained models, and counterfactual

analysis can convert correlations into testable hypotheses. Interpretable models have already demonstrated the possibility of deriving transferable descriptors for activity and selectivity across several electrocatalytic reactions, including CO_2 and nitrogen reduction (Lin *et al*., 2024). Explanations must nevertheless be validated experimentally because a statistically important feature is not automatically mechanistic.

Reliable datasets remain the primary bottleneck. Published electrocatalysis data are heterogeneous in electrode area, catalyst loading, reference-electrode calibration, electrolyte, cell design, iR correction, product analysis, and stability protocols. Negative results and synthesis failures are rarely reported, creating publication bias. Future databases should therefore follow findable, accessible, interoperable and reusable principles and record complete synthesis procedures, raw spectra, uncertainty, operating conditions, product balances, and failure modes. Chen *et al.,* (2024) demonstrated how natural-language processing and large language models can structure CO_2-electrocatalysis literature, producing corpora containing catalyst, synthesis, product, Faradaic-efficiency and operating-condition information. However, expert validation remains necessary because automated extraction is more reliable for explicit numerical entities than for descriptive or context-dependent information.

Standardized reporting would allow models trained in one laboratory to generalize to another. Common ontologies should connect catalyst identity, atomic coordination, electrode architecture, electrolyte, reactor, operando structure and product distribution. Data should retain provenance at every transformation, while benchmark datasets require version control, duplicate detection, uncertainty estimates and external test sets. Models intended for autonomous decisions should report applicability domains and calibrated uncertainty rather than single deterministic predictions.

Digital twins could integrate catalyst kinetics, mass transport, membrane behavior, degradation, separation and renewable-power availability. A working digital twin would be updated continuously by operando spectroscopy, electrochemical impedance, flow, temperature and product sensors. It could predict flooding, salt deposition, selectivity drift or metal dissolution and adjust pressure, potential, flow rate or regeneration schedules. Importantly, digital twins must incorporate conservation laws and electrochemical constraints, preventing AI-generated operating policies from violating physical or safety boundaries.

Autonomous laboratories complete the closed loop by coupling hypothesis generation, robotic synthesis, characterization, electrochemical testing and active learning. Burger *et al.,* (2020) demonstrated 688 autonomous photocatalysis experiments over eight days, illustrating how Bayesian optimization can explore multivariable chemical spaces efficiently. For SAC electrocatalysis, analogous systems must handle powders, inks, gas-diffusion electrodes, contamination-sensitive ammonia analysis and operando data. Human oversight will remain essential for defining objectives, auditing unexpected results and assessing sustainability. Ultimately, autonomous carbon-neutral manufacturing should optimize multiple objectives simultaneously activity, selectivity, lifetime, cost, energy efficiency and environmental burden rather than producing catalysts that maximize a single laboratory metric.

CONCLUSION

AI-guided single-atom electrocatalysis offers a compelling pathway for connecting renewable electricity with carbon-neutral chemical manufacturing. By maximizing metal utilization and enabling precise regulation of coordination structure, electronic configuration, and metal–support interactions, single-atom catalysts provide an adaptable platform for transforming waste-derived CO_2 and nitrate into valuable chemicals. Their combination with artificial intelligence can substantially accelerate catalyst discovery by predicting adsorption energetics, limiting potentials, reaction selectivity, stability, and experimentally relevant structure–performance relationships before extensive synthesis and testing. Nevertheless, realizing this potential requires the field to progress beyond isolated demonstrations of high Faradaic efficiency toward integrated materials, device, and process development.

For CO_2 electroreduction, Fe-, Co-, Ni-, Cu-, Zn-, Sn-, and Bi-based atomic sites can direct product formation toward CO, formate, hydrocarbons, or oxygenates through coordination and support engineering. However, producing multicarbon products remains difficult because isolated sites may not naturally provide the adjacent adsorption configurations required for carbon–carbon coupling. Dynamic aggregation, tandem sites, dual-atom configurations, and controlled interactions between single atoms and nanoparticles may address this limitation, but their working structures must be established through operando characterization. Nitrate-to-ammonia electroreduction presents a complementary route that integrates nitrogen recovery, wastewater remediation, and decentralized ammonia production. Its practical value depends on maintaining high ammonia selectivity across realistic nitrate concentrations while suppressing hydrogen evolution and undesired nitrogen-containing products.

AI can help navigate these multidimensional reaction spaces, although model reliability is governed by the quality and relevance of the underlying data. Heterogeneous reporting practices, incomplete metadata, publication bias, small datasets, and inconsistent definitions of active sites currently restrict model transferability. Future databases should therefore include

unsuccessful experiments, synthesis details, catalyst loading, reactor configuration, electrolyte composition, product concentrations, uncertainty estimates, operando structures, and durability data. Explainable and physics-informed models are particularly important because accurate predictions without chemically interpretable reasoning offer limited guidance for catalyst design.

Characterization must similarly evolve from static confirmation of atomic dispersion to identification of catalytically relevant working states. Combining HAADF-STEM, XPS, XANES, EXAFS, vibrational spectroscopy, Mössbauer spectroscopy, isotope labelling, online product analysis, and operando measurements can distinguish stable single atoms from reconstructed, dissolved, or aggregated species. Performance evaluation should prioritize product-specific current density, complete Faradaic and elemental balances, energy efficiency, product concentration, reproducibility, and long-duration operation under industrially meaningful conditions.

Ultimately, successful industrial translation will be determined not by catalyst activity alone but by full-cell voltage, durability, reactant utilization, separation requirements, renewable-electricity availability, manufacturing cost, and life-cycle environmental performance. Closed-loop autonomous laboratories and digital twins could integrate these objectives by continuously linking prediction, synthesis, characterization, electrochemical testing, process modelling, and sustainability assessment. Human oversight, transparent algorithms, standardized reporting, and rigorous experimental verification must remain central to this framework. Through such coordinated development, AI-guided single-atom electrocatalysts may evolve from promising laboratory materials into reliable components of autonomous, resource-efficient, and genuinely carbon-neutral chemical manufacturing systems.

REFERENCES

- Ahmad, H., Sarwar, M. A., Khan, A. N., Alvi, A., Riaz, U., Khawaja, L., Mudassar, M. A., Ahmad, A., Iltaf, & Khan, W. Z. (2025). Unified intelligence: A comprehensive review of the synergy between data science, artificial intelligence, and machine learning in the age of big data. *Scholars Journal of Engineering and Technology, 13*(8), 585–617. https://doi.org/10.36347/sjet.2025.v13i08.001
- Akhtar, M. A., Hussain, Z., Shareef, F., Khan, W. Z., Othi, N. A., Nawaz, A., Batool, A., Rubab, K., Maqsood, H., & Munir, F. (2024). Exploring the frontiers of material science for energy sustainability: Breakthroughs in batteries, smart electronics, renewable energy systems, and next-generation electric mobility solutions. *Global Scientific and Academic Research Journal of Multidisciplinary Studies, 3*(12), 9–24. https://doi.org/10.5281/zenodo.14268208
- Ashraf, M. R., Hazim, M., Khawaja, L., Sundhu, M. U., Sattar, N., Afzal, A., Danyal, M. M., Bibi, S., Iltaf, & Khan, W. Z. (2025). Intelligent science, one world: A pan-disciplinary review of data science, Python, machine learning and AI across big data, cloud–edge and HPC/quantum, IoT and robotics, cybersecurity, bio/health informatics, geospatial/remote sensing, blockchain, digital twins, and responsible governance. *Scholars Journal of Engineering and Technology, 13*(12), 915–930. https://doi.org/10.36347/sjet.2025.v13i12.006
- Aslam, E. E., Khan, W. Z., Mudassar, M. A., Yousaf, U., Hussain, A., Aslam, S., & Majeed, T. (2025). Light–matter strategies for next-generation solar cells: Active-medium architectures, ultrafast carrier dynamics, and laser-enabled photonic structuring. *Scholars Journal of Physics, Mathematics and Statistics, 12*(10), 435–467. https://doi.org/10.36347/sjpms.2025.v12i10.001
- Bae, G., Kim, H., Choi, H., & Lee, H. (2023). Operando stability of single-atom electrocatalysts. *Angewandte Chemie International Edition, 62*(19), e202219227. DOI: 10.1002/anie.202219227
- Bagemihl, I., Cammann, L., Pérez-Fortes, M., van Steijn, V., & van Ommen, J. R. (2023). Techno-economic assessment of CO_2 electrolysis: How interdependencies between model variables propagate across different modeling scales. *ACS Sustainable Chemistry & Engineering, 11*. DOI: 10.1021/acssuschemeng.3c02226
- Belsa, B., Xia, L., & García de Arquer, F. P. (2024). CO_2 electrolysis technologies: Bridging the gap toward scale-up and commercialization. *ACS Energy Letters, 9*(9), 4293–4305. DOI: 10.1021/acsenergylett.4c00955
- Bennett, J. A., Tarzia, A., Lovelock, S. L., *et al.,* (2024). Autonomous reaction Pareto-front mapping with a self-driving catalysis laboratory. *Nature Chemical Engineering, 1*, 240–250. DOI: 10.1038/s44286-024-00033-5
- Birdja, Y. Y., Pérez-Gallent, E., Figueiredo, M. C., Göttle, A. J., Calle-Vallejo, F., & Koper, M. T. M. (2021). Advances and challenges in understanding the electrocatalytic conversion of carbon dioxide to fuels. *Nature Energy, 6*, 732–745. DOI: 10.1038/s41560-021-00846-x
- Burger, B., Maffettone, P. M., Gusev, V. V., Aitchison, C. M., Bai, Y., Wang, X., Li, X., Alston, B. M., Li, B., Clowes, R., Rankin, N., Harris, B., Sprick, R. S., & Cooper, A. I. (2020). A mobile robotic chemist. *Nature, 583*(7815), 237–241. DOI: 10.1038/s41586-020-2442-2
- Cai, J., Wei, Y., Cao, A., Huang, J., Jiang, Z., Lu, S., & Zang, S. Q. (2022). Electrocatalytic nitrate-to-ammonia conversion with approximately 100% Faradaic efficiency via single-atom alloying. *Applied Catalysis B: Environmental, 316*, 121683. DOI: 10.1016/j.apcatb.2022.121683

- Chen, C., Li, J., Tan, X., Zhang, Y., Li, Y., He, C., Xu, Z., Zhang, C., & Chen, C. (2024). Harnessing single-atom catalysts for CO_2 electroreduction: A review of recent advances. *EES Catalysis, 2*, 71–93. DOI: 10.1039/D3EY00150D
- Chen, X., Gao, Y., Wang, L., Cui, W., Huang, J., Du, Y., & Wang, B. (2024). Large language model enhanced corpus of CO_2 reduction electrocatalysts and synthesis procedures. *Scientific Data, 11*, 347. DOI: 10.1038/s41597-024-03180-9
- Chen, Y., *et al.,* (2024). Electrocatalytic nitrate reduction: The synthesis, recovery and sustainable utilization of ammonia. *Journal of Environmental Chemical Engineering, 12*, 112233.
- Chen, Z. W., Lu, Z., Chen, L. X., Jiang, M., Chen, D., & Singh, C. V. (2021). Machine-learning-accelerated discovery of single-atom catalysts based on bidirectional activation mechanism. *Chem Catalysis, 1*(1), 183–195. DOI: 10.1016/j.checat.2021.03.003
- Ding, Z., Pang, Y., Ma, A., Liu, Z., Wang, Z., Fan, G., & Xu, H. (2024). Single-atom catalysts based on two-dimensional metalloporphyrin monolayers for electrochemical nitrate reduction to ammonia by first-principles calculations and interpretable machine learning. *International Journal of Hydrogen Energy, 80*, 1050–1061.
- Dong, J., Liu, Y., Pei, J., Li, H., Ji, S., Shi, L., Zhang, Y., Li, C., Tang, C., Liao, J., Xu, S., Zhang, H., Li, Q., & Zhao, S. (2023). Continuous electroproduction of formate via CO_2 reduction on local symmetry-broken single-atom catalysts. *Nature Communications, 14*, 6849. DOI: 10.1038/s41467-023-42539-1
- Eryazici, I., Ramesh, N., & Villa, C. (2021). Electrification of the chemical industry—Materials innovations for a lower carbon future. *MRS Bulletin, 46*(12), 1197–1204. DOI: 10.1557/s43577-021-00243-9
- Farghali, M., *et al.,* (2024). Strategies for ammonia recovery from wastewater: A review. *Environmental Chemistry Letters, 22*, 2689–2722. DOI: 10.1007/s10311-024-01768-6
- Finzel, J., Kube, P., Hönig, D., Willinger, M. G., & Trunschke, A. (2023). Limits of detection for EXAFS characterization of heterogeneous single-atom catalysts. *ACS Catalysis, 13*. DOI: 10.1021/acscatal.3c01116
- Gabrielli, P., Rosa, L., Gazzani, M., Meys, R., Bardow, A., Mazzotti, M., & Sansavini, G. (2023). Net-zero emissions chemical industry in a world of limited resources. *One Earth, 6*(6), 682–704. DOI: 10.1016/j.oneear.2023.05.006
- Gao, J., *et al.,* (2022). Electrocatalytic upcycling of nitrate wastewater into an ammonia fertilizer. *Environmental Science & Technology, 56*, 11602–11613. DOI: 10.1021/acs.est.1c08442
- Gao, J., *et al.,* (2023). Electrocatalytic reduction of nitrate to ammonia via a Au/Cu single-atom alloy catalyst. *Environmental Science & Technology, 57*, 4010–4019. DOI: 10.1021/acs.est.2c07968
- Ghanekar, P. G., Deshpande, S., & Greeley, J. (2022). Adsorbate chemical environment-based machine learning framework for heterogeneous catalysis. *Nature Communications, 13*, 5788. DOI: 10.1038/s41467-022-33256-2
- Giulimondi, V., Mitchell, S., & Pérez-Ramírez, J. (2023). Challenges and opportunities in engineering the electronic structure of single-atom catalysts. *ACS Catalysis, 13*(5), 2981–2997. DOI: 10.1021/acscatal.2c05992
- Guerra, O. J., Almajed, H. M., Smith, W. A., Somoza-Tornos, A., & Hodge, B.-M. S. (2023). Barriers and opportunities for the deployment of CO_2 electrolysis in net-zero emissions energy systems. *Joule, 7*(6), 1111–1133. DOI: 10.1016/j.joule.2023.05.002
- Halder, D., *et al.,* (2025). Recent advances in mechanistic studies and catalyst development for electrochemical nitrate reduction to ammonia. *Communications Chemistry, 8*, 24. DOI: 10.1038/s42004-025-01864-w
- Han, C., Zhang, S., Zhang, H., Dong, Y., Yao, P., Du, Y., Song, P., Gong, X., & Xu, W. (2024). Metal–support interaction in single-atom electrocatalysts: A perspective of metal oxide supports. *eScience, 4*(5), 100269. DOI: 10.1016/j.esci.2024.100269
- Han, L., Song, S., Liu, M., Yao, S., Liang, Z., Cheng, H., Ren, Z., Liu, W., Lin, R., Qi, G., Liu, X., Wu, Q., Luo, J., & Xin, H. L. (2020). Stable and efficient single-atom Zn catalyst for CO_2 reduction to CH_4. *Journal of the American Chemical Society, 142*, 12563–12567. DOI: 10.1021/jacs.9b12111
- Huang, H., *et al.,* (2024). Rethinking nitrate reduction: Redirecting electrochemical strategies from pollutant removal to ammonia recovery. *Energy & Environmental Science, 17*, 2682–2702.
- Huang, J.-R., Qiu, X.-F., Zhao, Z.-H., Zhu, H.-L., Liu, Y.-C., Shi, W., Liao, P.-Q., & Chen, X.-M. (2022). Single-product Faradaic efficiency for electrocatalytic CO_2 to CO at current density larger than 1.2 A cm^{-2} in neutral aqueous solution by a single-atom nanozyme. *Angewandte Chemie International Edition, 61*, e202210985. DOI: 10.1002/anie.202210985
- Hussain, S., Yasmin, R., Chouhdary, A. N., Irfan, M., Munir, F., Ahmad, S., Afzal, M., Liaqat, M., Ibrahim, U., & Khan, W. Z. (2025). From atomic nuclei to nanostructures: Harnessing the convergence of nuclear physics, particle dynamics, and nanotechnology to transform energy, revolutionize medicine, and advance environmental sustainability. *Global Scientific and Academic Research Journal of Multidisciplinary Studies, 4*(1), 87–117. https://doi.org/10.5281/zenodo.14789142
- Iqbal, M. T., Saeeda, S., Zahra, T., Umar, Z., Khan, W. Z., Adnan, M., Raza, H., Shah, G. A., &

Toffique, M. (2025). Next-generation materials discovery using DFT: Functional innovation, solar energy, catalysis, and ecotoxicity modelling. *Scholars Journal of Engineering and Technology, 13*(7), 454–486. DOI: 10.36347/sjet.2025.v13i07.003

- Iqbal, M. T., Saeeda, S., Zahra, T., Umar, Z., Khan, W. Z., Adnan, M., Raza, H., Shah, G. A., & Toffique, M. (2025). Next-generation materials discovery using DFT: Functional innovation, solar energy, catalysis, and ecotoxicity modelling. *Scholars Journal of Engineering and Technology, 13*(7), 454–486. https://doi.org/10.36347/sjet.2025.v13i07.003
- Jabeen, N., Naseem, A., Sarfraz, M., Murtaza, M., Ali, T., Haq, M. U., Farooq, M. U., Shabbir, A., Hameed, F., & Khan, W. Z. (2025). Cross-disciplinary research gaps in physical, chemical, and environmental sciences: An integrative review from nanotechnology to wastewater treatment, renewable energy, artificial intelligence, and biomedical engineering. *Scholars Journal of Physics, Mathematics and Statistics, 12*(9), 369–388. https://doi.org/10.36347/sjpms.2025.v12i09.001
- Jenewein, K. J., Boubnov, A., Gänzler, A. M., *et al.,*(2024). Multiobjective Bayesian optimization of non-noble acidic oxygen evolution electrocatalysts. *Journal of Materials Chemistry A, 12*, 6684–6694. DOI: 10.1039/D3TA06651G
- Kempler, P. A., & Nielander, A. C. (2023). Reliable reporting of Faradaic efficiencies for electrocatalysis research. *Nature Communications, 14*, 1158. DOI: 10.1038/s41467-023-36880-8
- Khan, S., Ali, F., Khan, W. Z., Adnan, M., Naveed, R. M. J., Rasool, B., Ayub, U., Adeel, M., & Malik, M. R. (2025). AI-driven and quantum-informed design of functional nanomaterials: Bridging catalysis, drug discovery, and sustainable environmental remediation. *Scholars Journal of Physics, Mathematics and Statistics, 12*(9), 389–418. https://doi.org/10.36347/sjpms.2025.v12i09.002
- Khan, U. U., Umair, M., Zahid, A. H., Aziz, M., Kharl, M. U. F. A., Aftab, M., Sayam, H., Farooq, M. U., Hassan, S., & Khan, W. Z. (2026). AI and physics-guided multimodal chemical measurement: Unifying spectroscopy, chromatography–mass spectrometry, electrochemical sensing, and chemical imaging via data fusion from molecules to materials and devices. *Scholars Journal of Engineering and Technology, 14*(1), 10–40. https://doi.org/10.36347/sjet.2026.v14i01.002
- Khan, W. Z. (2025). Role of spin-orbit coupling in Bi-rich to In-rich $Cs_2Ag(In_xBi_{1-x})Cl_6$: Electronic and optical design by DFT. *Computational Materials Science*. https://doi.org/10.1016/j.commatsci.2025.11427
- Khan, W. Z., Fatima, M., Ahmad, S., Afzal, M., Rafique, S., Ali, A., Tabassam, M. N., & Akram, I. (2025). Advancing diagnostic medical physics: AI, MR-guided radiotherapy, and 3D printing in modern healthcare. *Dialogue Social Science Review, 3*(1), 1–25. https://dialoguessr.com/index.php/2/article/view/140
- Khan, W. Z., Haseeb, M., Khan, S. N., Falk, M., Liaqat, M., Akhtar, W., & Ahmad, S. (2025). Quantum materials: Key to advancing quantum computing by enhancing stability, scalability, and error resistance through superconductors, topological insulators, and 2D materials for scalable systems. *Global Scientific and Academic Research Journal of Multidisciplinary Studies, 4*(4), 1–30. https://doi.org/10.5281/zenodo.15180740
- Khan, W. Z., Ishfaq, A., Akhtar, A., Abdullah, & Ahmad, I. (2026). Sensorless thermometry from MPPT electrical traces: A physics-informed inversion for perovskite solar cells. *Scholars Journal of Physics, Mathematics and Statistics, 13*(4), 150–165. https://doi.org/10.36347/sjpms.2026.v13i04.001
- Khan, W. Z., Nazar, M., Younis, B., Mahnoor, Akbar, H., Ahmad, S., Rustam, R., Akram, I., & Munir, F. (2024). Advancing perovskite solar cells: Addressing stability, scalability, and environmental challenges. *Dialogue Social Science Review, 2*(4), 395–422. https://dialoguesreview.com/index.php/2/article/view/82
- Khan, W. Z., Yasmin, R., Akbar, H., Irfan, M., Noor, G. M., Ali, H., Ahmad, I., Ibrahim, U., & Anwar, A. (2025). Advancements in laser technology: Bridging historical milestones and modern applications in science, industry, and sustainability. *Global Scientific and Academic Research Journal of Multidisciplinary Studies, 4*(1), 70–84. https://doi.org/10.5281/zenodo.14770605
- Kottwitz, M., Li, Y., Wang, H., Frenkel, A. I., & Nuzzo, R. G. (2021). Single atom catalysts: A review of characterization methods. *Chemistry—Methods, 1*, 278–294. DOI: 10.1002/cmtd.202100020
- Leghari, H. M., Shah, I. H., Shahzad, F., Haq, I. U., Mudassar, M. A., Ashfaq, F., Ghazal, H., Munawar, A., Shehzadi, S., & Khan, W. Z. (2025). Enhancing perovskite solar cell efficiency via tunable Ag nanoparticle-integrated SnO_2 transport layers: Mechanistic insights and air-fabrication approach. *Scholars Journal of Physics, Mathematics and Statistics, 12*(7), 254–267. https://doi.org/10.36347/sjpms.2025.v12i07.002
- Lin, X., *et al.,* (2024). Machine-learning-assisted dual-atom-site design with an interpretable descriptor for multiple electrocatalytic reactions. *Nature Communications, 15*. DOI: 10.1038/s41467-024-52519-8
- Lu, Z., Liu, J., Li, H., Li, R., Zhang, X., Jian, X., Gao, X., Zhang, X., Wu, Y., & Yue, X. (2025).

Leveraging machine learning to expedite screening of single-atom catalysts in electrochemical nitrate reduction to ammonia. *Journal of Alloys and Compounds, 1010*, 177180. DOI: 10.1016/j.jallcom.2024.177180

- Luo, J., Waterhouse, G. I. N., Peng, L., & Chen, Q. (2023). Recent progress in high-loading single-atom catalysts and their applications. *Industrial Chemistry & Materials, 1*(4), 486–500. DOI: 10.1039/D3IM00062A
- Ma, M., Clark, E. L., Therkildsen, K. T., Dalsgaard, S., Chorkendorff, I., & Seger, B. (2020). Insights into the carbon balance for CO_2 electroreduction on Cu using gas diffusion electrode reactor designs. *Energy & Environmental Science, 13*, 977–985. DOI: 10.1039/C9EE03761B
- Malik, A., Liaqat, M., Rahman, M. U., Shafique, A. Y., Haseeb, M., Ahmad, S., Kanwal, R., Ramzan, M., Yasmin, R., & Khan, W. Z. (2025). Nanotechnology for perovskite solar cells: Solving efficiency, stability, and energy-storage challenges. *Global Scientific and Academic Research Journal of Multidisciplinary Studies, 4*(2), 68–89. https://doi.org/10.5281/zenodo.14913631
- Mallapragada, D. S., Dvorkin, Y., Modestino, M. A., Esposito, D. V., Smith, W. A., Hodge, B.-M., Harold, M. P., Donnelly, V. M., Nuz, A., Bloomquist, C., Baker, K., Grabow, L. C., Yan, Y., Rajput, N. N., Hartman, R. L., Biddinger, E. J., Aydil, E. S., & Taylor, A. D. (2023). Decarbonization of the chemical industry through electrification: Barriers and opportunities. *Joule, 7*(1), 23–41. DOI: 10.1016/j.joule.2022.12.008
- Martini, A., Borfecchia, E., Lomachenko, K. A., *et al.,* (2023). Tracking the evolution of single-atom catalysts for the CO_2 electroreduction using operando X-ray absorption spectroscopy and machine learning. *Journal of the American Chemical Society, 145*, 17351–17366. DOI: 10.1021/jacs.3c04826
- Martini, A., Hursán, D., Timoshenko, J., Rüscher, M., Haase, F., Rettenmaier, C., Ortega, E., Etxebarria, A., & Roldan Cuenya, B. (2023). Tracking the evolution of single-atom catalysts for the CO_2 electrocatalytic reduction using operando X-ray absorption spectroscopy and machine learning. *Journal of the American Chemical Society, 145*, 17351–17366. DOI: 10.1021/jacs.3c04826
- Mudassar, M. A., Khalid, A., Ashraf, A., Barkat, U., Aslam, M. A., Talha, H. M., Abdullah, M., Munawar, A., Ghazal, H., & Khan, W. Z. (2025). Theoretical design and optoelectronic analysis of lead-free $CsPbX_3/Cs_2SnX_6$ core–shell perovskite nanocrystals for enhanced stability and charge dynamics. *Scholars Journal of Physics, Mathematics and Statistics, 12*(6), 226–239. https://doi.org/10.36347/sjpms.2025.v12i06.004
- Nazar, M., Tabassam, M. N., Irfan, A., Liaqat, M., Ameen, M., Chaudhary, H. M., Murad, K., Alam, S., Sohaib, M., & Khan, W. Z. (2025). DFT study of optoelectronic and thermoelectric properties of halide double perovskite Rb_2TlSbX_6 (X = Cl, Br, I) for solar-cell applications. *Scholars Journal of Engineering and Technology, 13*(4), 208–222. https://doi.org/10.36347/sjet.2025.v13i04.002
- Nitopi, S., Bertheussen, E., Scott, S. B., *et al.,*(2021). Progress and perspectives of electrochemical CO_2 reduction on copper in aqueous electrolyte. *Chemical Reviews, 121*, 12497–12580. DOI: 10.1021/acs.chemrev.1c00261
- Niu, H., Zhang, Z., Wang, X., Wan, X., Shao, C., & Guo, Y. (2021). Theoretical insights into the mechanism of selective nitrate-to-ammonia electroreduction on single-atom catalysts. *Advanced Functional Materials, 31*, 2008533. DOI: 10.1002/adfm.202008533
- Nwabara, U. O., de Heer, M. P., Cofell, E. R., Verma, S., Negro, E., & Kenis, P. J. A. (2020). Towards accelerated durability testing protocols for CO_2 electrolysis. *Journal of Materials Chemistry A, 8*(43), 22557–22571. DOI: 10.1039/D0TA08695A
- Pablo-García, S., Morandi, S., Vargas-Hernández, R. A., Jorner, K., Ivković, Ž., López, N., & Aspuru-Guzik, A. (2023). Fast evaluation of the adsorption energy of organic molecules on metals via graph neural networks. *Nature Computational Science, 3*, 433–442. DOI: 10.1038/s43588-023-00437-y
- Pan, Q., Zhang, Y., Yang, C., *et al.,*(2023). Insight into the active sites of M–N–C single-atom catalysts for electrochemical CO_2 reduction. *Carbon Energy, 5*, e287. DOI: 10.1002/cey2.287
- Park, W., Noh, J., Gu, G. H., Nam, G., Jung, S.-M., Kim, Y.-T., & Jung, Y. (2024). Machine learning-enabled fast exploration of stable and active single-atom catalysts for oxygen evolution reaction. *The Innovation Materials, 2*(2), 100072. DOI: 10.59717/j.xinn-mater.2024.100072
- Qi, P., Wang, J., Djitcheu, X., He, D., Liu, H., & Zhang, Q. (2022). Techniques for the characterization of single-atom catalysts. *RSC Advances, 12*, 1216–1227. DOI: 10.1039/D1RA076atomically dispersed catalyst characterization article
- Qi, R., Zhu, B., Han, Z., & Gao, Y. (2022). High-throughput screening of stable single-atom catalysts in CO_2 reduction reactions. *ACS Catalysis, 12*(14), 8269–8278. DOI: 10.1021/acscatal.2c02149
- Qian, S., Zhao, Z., Chen, Y., *et al.,*(2024). Tailoring coordination environments of single-atom electrocatalysts for hydrogen evolution by topological heteroatom transfer. *Nature Communications, 15*, 2774. DOI: 10.1038/s41467-024-47061-6
- Rafiq, M. N., Liaqat, M., Sadiqa, M., Shams, H., Farrukh, M., Sarfraz, R., Rehman, M. U., & Khan, W. Z. (2025). Enhanced dielectric and piezoelectric properties of $BaTiO_3$-infused $K_{0.3}Na_{0.2}Bi_{0.5}TiO_3$ ceramics for high-frequency applications. *Global*

Scientific and Academic Research Journal of Multidisciplinary Studies, 4(2), 94–100. https://doi.org/10.5281/zenodo.14956707

- Raman, G., *et al.,* (2025). A machine-learning approach for prediction of Faradaic efficiency in electrochemical CO_2 reduction. *ChemPlusChem, 90*, e202400766. DOI: 10.1002/cplu.202400766
- Schilter, O., Vaucher, A. C., Schwaller, P., *et al.,*(2024). Combining Bayesian optimization and automation to simultaneously optimize reaction conditions for multiple substrates. *Chemical Science, 15*, 3766–3775. DOI: 10.1039/D3SC05607D
- Seger, B., Robert, M., & Jiao, F. (2023). Best practices for electrochemical reduction of carbon dioxide. *Nature Sustainability, 6*(3), 236–238. DOI: 10.1038/s41893-022-01034-z
- Shafique, A. Y., Nazar, M., Liaqat, M., Khan, F. A., Ahmad, S., & Khan, W. Z. (2025). Synthesis and characterization of La-doped BNBT lead-free ceramics with enhanced piezoelectric and dielectric properties. *Global Scientific and Academic Research Journal of Multidisciplinary Studies, 4*(2), 56–67. https://doi.org/10.5281/zenodo.15046638
- Shah, I. H., Anjum, I., Javed, L., Yousaf, W., Liaqat, I., Khan, M. Y., Attique, L., & Khan, W. Z. (2026). A cross-scale design grammar for functional matter: Integrating synthetic pathways, reaction mechanisms, self-assembly, interfaces, defect chemistry, multimodal characterization, predictive modeling, and performance validation. *Scholars International Journal of Chemistry and Material Sciences, 9*(2), 77–100. https://doi.org/10.36348/sijcms.2026.v09i02.002
- Shah, I. H., Khan, M. Y., Khan, W. Z., & Hameed, K. (2026). Variational, B(R)-independent bounds for photon spheres and black-hole shadows: Existence, stability, tight inequalities, and observation-ready predictions. *Scholars Journal of Physics, Mathematics and Statistics, 13*(3), 118–132. https://doi.org/10.36347/sjpms.2026.v13i03.004
- Shakeel, R., Ahmad, A., Mushtaq, H., Haider, T., Javeria, M., Asif, A., Zia, K., Zafar, H., Ishaque, B., & Khan, W. Z. (2025). Multifunctional nanomaterials in materials chemistry: A cross-disciplinary review of applications in energy, environment, catalysis, and biomedicine. *Scholars Journal of Engineering and Technology, 13*(8), 673–707. https://doi.org/10.36347/sjet.2025.v13i08.007
- Sharjeel, M., Tariq, S., Ahmad, M., Aslam, A., Iltaf, Khawaja, L., Jameel, A., Shah, S. A., Ahmad, M., & Khan, W. Z. (2025). An interdisciplinary review of modern computer science: Trends and challenges in AI, cybersecurity, cloud, blockchain, IoT, data science, NLP, vision, software engineering, and quantum computing. *Scholars Journal of Engineering and Technology, 13*(9), 768–793. https://doi.org/10.36347/sjet.2025.v13i09.005
- Shields, B. J., Stevens, J., Li, J., Parasram, M., Damani, F., Alvarado, J. I. M., Janey, J. M., Adams, R. P., & Doyle, A. G. (2021). Bayesian reaction optimization as a tool for chemical synthesis. *Nature, 590*, 89–96. DOI: 10.1038/s41586-021-03213-y
- Song, W., Xiao, C., Ding, J., Huang, Z., Yang, X., Zhang, T., Mitlin, D., & Hu, W. (2024). Review of carbon support coordination environments for single metal atom electrocatalysts. *Advanced Materials, 36*(1), 2301477. DOI: 10.1002/adma.202301477
- Song, Z., *et al.,* (2025). Inverse design of promising electrocatalysts for CO_2 reduction through a generative artificial-intelligence framework. *Nature Communications, 16*, 300. DOI: 10.1038/s41467-024-55613-z
- Su, Y., Wang, X., Ye, Y., Xie, Y., Xu, Y., Jiang, Y., & Wang, C. (2024). Automation and machine learning augmented by large language models in a catalysis study. *Chemical Science, 15*, 12200–12233. DOI: 10.1039/D3SC07012C
- Subhadarshini, S., *et al.,* (2024). Single-atom catalyst for nitrate-to-ammonia electrochemistry. *Small, 20*, 2403515. DOI: 10.1002/smll.202403515
- Tabassam, M. N., Haseeb, M., Habib, M. A. B., Murtaza, R., Ali, S., Malik, M. R., Numan, M., Mahmood, M., Mustafa, Z., & Khan, W. Z. (2025). Next-generation adsorbents for wastewater remediation: A nanotechnology-driven and AI-enabled breakthrough towards clean water. *Scholars Journal of Physics, Mathematics and Statistics, 12*(8), 323–345. https://doi.org/10.36347/sjpms.2025.v12i08.001
- Tamtaji, M., Chen, S., Hu, Z., Goddard, W. A., III, & Chen, G. (2023). A surrogate machine learning model for the design of single-atom catalyst on carbon and porphyrin supports towards electrochemistry. *The Journal of Physical Chemistry C, 127*, 9992–10000. DOI: 10.1021/acs.jpcc.3c00765
- Tom, G., Schmid, S. P., Baird, S. G., *et al.,* (2024). Self-driving laboratories for chemistry and materials science. *Chemical Reviews, 124*, 9633–9732. DOI: 10.1021/acs.chemrev.4c00055
- van Langevelde, P. H., Katsounaros, I., & Koper, M. T. M. (2021). Electrocatalytic nitrate reduction for sustainable ammonia production. *Joule, 5*(2), 290–294. DOI: 10.1016/j.joule.2020.12.025
- Wang, H., Liu, W., Qi, J., Li, Q., & Wang, X. (2025). Structural evolution of metal single atoms and clusters in catalysis: Which are the active sites under operative conditions? *Chemical Science, 16*, 6203–6218. DOI: 10.1039/D5SC01221J
- Wang, S., Liu, C., Hao, W., Zhuang, Y., Chen, J., Zhu, X., Wang, L., Niu, X., Mao, J., Ma, D., & Zhao, Q. (2025). Structural evolution of metal single-atoms and clusters in catalysis: Which are the active

sites under operative conditions? *Chemical Science, 16*, 6203–6218. DOI: 10.1039/D5SC01221J

- Wu, Y., Wang, R., & Kim, Y. (2024). Single-atom catalysts on covalent organic frameworks for energy applications. *ACS Applied Materials & Interfaces, 16*(49), 66874–66899. DOI: 10.1021/acsami.3c17662
- Wu, Z.-Y., Karamad, M., Yong, X., *et al.,*(2021). Electrochemical ammonia synthesis via nitrate reduction on Fe single-atom catalyst. Nature Communications, 12, 2870. DOI: 10.1038/s41467-021-23115-x
- Xi, S., Zhao, P., He, C., & Zhang, W. (2024). High-throughput screening of single-atom catalysts on 1T-TMD for highly active and selective CO_2 reduction reaction: Computational and machine learning insights. Journal of Catalysis, 436, 115610. DOI: 10.1016/j.jcat.2024.115610
- Xia, R., Overa, S., & Jiao, F. (2022). Emerging electrochemical processes to decarbonize the chemical industry. JACS Au, 2(5), 1054–1070. DOI: 10.1021/jacsau.2c00138
- Zahid, T., Shakeel, R., Rehman, H. M. A., Rafique, S., Ali, T., Parvaiz, M., Kashif, M., Anjum, S., Shah, S. M. W., & Khan, W. Z. (2025). Brain-targeted delivery and redox-responsive release of protein therapeutics via GSH-sensitive SiO_2 nanoparticles.
- *Annual Methodological Archive Research Review, 3*(7), 648–675. https://doi.org/10.63075/j1p31406
- Zeng, Y., Li, X., Wang, J., Sougrati, M. T., Huang, Y., Zhang, T., & Liu, B. (2021). In situ/operando Mössbauer spectroscopy for probing heterogeneous catalysis. Chem Catalysis, 1, 1215–1233. DOI: 10.1016/j.checat.2021.08.013
- Zhang, K., Liu, Y., Pan, Z., Xia, Q., Huo, X., Esan, O. C., Zhang, X., & An, L. (2024). Cu-based catalysts for electrocatalytic nitrate reduction to ammonia: Fundamentals and recent advances. EES Catalysis, 2, 727–752. DOI: 10.1039/D4EY00002A
- Zheng, X., Li, P., Dou, S., Sun, W., Pan, H., Wang, D., & Li, Y. (2021). Non-carbon-supported single-atom site catalysts for electrocatalysis. Energy & Environmental Science, 14(5), 2809–2858. DOI: 10.1039/D1EE00248A
- Zubair, M. T. B., Khan, W. Z., Abbas, H., Asif, M., Ahmad, S., Abdullah, M., Adnan, M., Zafar, H., Ahmad, I., & Islam, S. U. (2025). First demonstration of lead-free double perovskite Cs_2NaBiI_6 as a dual-function electrode for high-performance, long-life photo-rechargeable lithium-ion batteries with superior solar-to-power conversion. *Scholars Journal of Physics, Mathematics and Statistics, 12*(8), 346–356. https://doi.org/10.36347/sjpms.2025.v12i08.002